NATIONAL ENERGY TECHNOLOGY LABORATORY

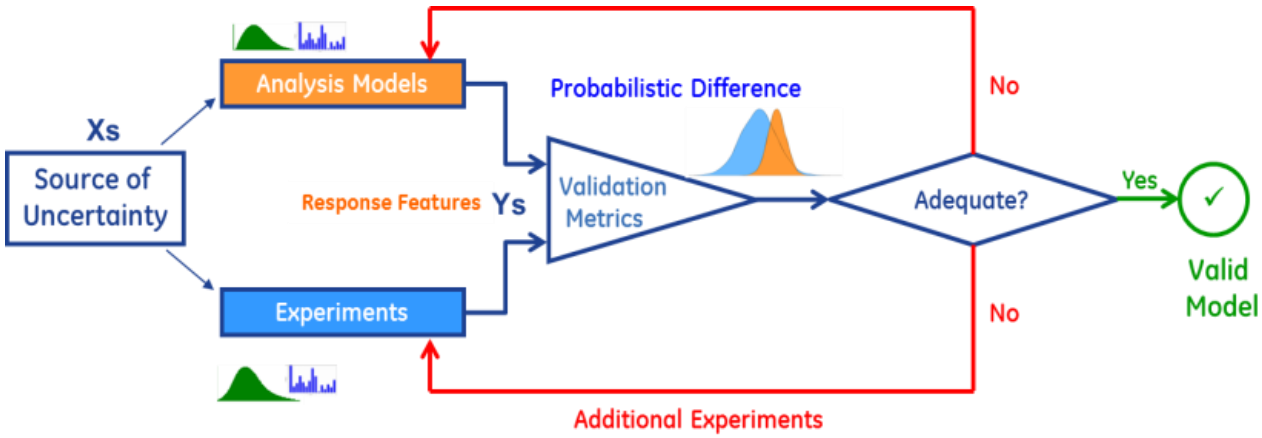

Uncertainty Quantification Analysis of Both Experimental and CFD Simulation Data of a Bench-scale Fluidized Bed Gasifier

2 October 2017

U.S. DEPARTMENT OF ENERGY | NATIONAL ENERGY TECHNOLOGY LABORATORY

Office of Fossil Energy

NETL-PUB-21341

Disclaimer

Cover Illustration: Workflow of approach required for quantifying uncertainty in both experimental and numerical data

Suggested Citation: Shahnam, M.; Gel, A.; Subramaniyan, A. K.; Musser, J.; Dietiker, J. F. *Title Uncertainty Quantification Analysis of Both Experimental and CFD Simulation Data of a Bench-scale Fluidized Bed Gasifier*; NETL-PUB-21341; NETL Technical Report Series; U.S. Department of Energy, National Energy Technology Laboratory: Morgantown, WV, 2017; p 68.

An electronic version of this report can be found at:

http://netl.doe.gov/research/on-site-research/publications/featured-technical-reports

https://edx.netl.doe.gov/carbonstorage

Uncertainty Quantification Analysis of Both Experimental and CFD Simulation Data of a Bench-scale Fluidized Bed Gasifier

Mehrdad Shahnam[1], Aytekin Gel[2], Arun K. Subramaniyan[3], Jordan Musser[4], Jean-Francois Dietiker[5]

[1] Energy Conversion Engineering Directorate, Research and Innovation Center, U.S. Department of Energy, National Energy Technology Laboratory, 3610 Collins Ferry Road, Morgantown, WV 26507

[2] ALPEMI Consulting, L.L.C., Phoenix, AZ 85048

[3] GE Global Research Center, Niskayuna, NY 12309

[4] Energy Conversion Engineering Directorate, Research and Innovation Center, U.S. Department of Energy, National Energy Technology Laboratory, 3610 Collins Ferry Road, Morgantown, WV 26507

[5] West Virginia University Research Corporation, Morgantown, WV 26505

NETL-PUB-21341

02 10 2017

NETL Contacts:

Mehrdad Shahnam, Principal Investigator

William A. Rogers, Technical Portfolio Lead

David Allman, Executive Director, Research and Innovation Center

This page intentionally left blank

Table of Contents

List of Figures

List of Tables

Acronyms, Abbreviations, and Symbols

Term	Description
DEM	Discrete Element Method
eCDF	empirical cumulative density function
FFT	Fast Fourier Transform
GP	Gaussian Processes
GPM	Gaussian Processes Model
GE	General Electric
GEBHM	General Electric Bayesian Hybrid Modeling
HPC	High Performance Computing
LANL	Los Alamos National Laboratory
MCMC	Markov Chain Monte Carlo
MPI	Message Passing Interface
MFiX	Multiphase Flow with Interphase Exchanges
MPPIC	Multiphase Particle in-Cell
NERSC	National Energy Research Scientific Computing
OLH	Optimal Latin Hypercube
PDF	probability density function
RSM	Response Surface Methodology
QoI	quantity of interest
TFM	Two Fluid Model
UQ	Uncertainty Quantification
β_δ	Discrepancy scaling parameter
β_η	Simulation response scaling parameter

δ	Discrepancy between test and simulation
ϵ	Measurement error
η	Output response from simulation model
$\widehat{\theta}$	True value of calibration parameters
$\hat{y}(x)$	Discrepancy updated model
$\lambda_{\delta Z}$	Precision of discrepancy response (marginal)
$\lambda_{\eta S}$	Precision of simulation response (marginal)
$\lambda_{\eta Z}$	Precision of simulation response
$\pi(.)$	Probability density distribution function
Σ	Covariance matrix
Σ_{δ}	Covariance matrix for discrepancy Gaussian Process Model
Σ_{η}	Covariance matrix for simulation Gaussian Process Model
Σ_{sim}	Covariance matrix for simulations
Σ_{test}	Covariance matrix for observations from experiments
Σ_{y}	Covariance matrix for observation Gaussian Process Model
θ	Calibration parameters
θ^{*}	Prior mean values of the calibration parameters
D	Combined model representation of data and discrepancy
L	Likelihood function
m	Number of simulation data
N	Number of output responses
n	Number of measured (experimental or test) data
x	Input, design parameters
y	Output responses (test data)

Acknowledgments

This work was completed as part of National Energy Technology Laboratory (NETL) research for the U.S. Department of Energy's (DOE) Advance Gasification Program under the RES contract DE-FE0004000. This work is also a joint effort between NETL and General Electric Global Research Center (GEGRC) performed under a cooperative research and development agreement (CRADA) No. AGMT-0407.

Portion of computational resources used in this research was provided through the 2014 and 2015 ASCR Leadership Computing Challenge (ALCC) program at the National Energy Research Scientific Computing Center (NERSC), a DOE Office of Science User Facility supported by the Office of Science of the U.S. Department of Energy under Contract No. DE-AC02-05CH11231, and Argonne Leadership Computing Facility (ALCF) at Argonne National Laboratory, respectively.

ABSTRACT

Adequate assessment of the uncertainties in modeling and simulation is becoming an integral part of the simulation based engineering design. The goal of this study is to demonstrate the application of non-intrusive Bayesian uncertainty quantification (UQ) methodology in multiphase (gas-solid) flows with experimental and simulation data, as part of our research efforts to determine the most suited approach for UQ of a bench scale fluidized bed gasifier. UQ analysis was first performed on the available experimental data. Global sensitivity analysis performed as part of the UQ analysis shows that among the three operating factors, steam to oxygen ratio has the most influence on syngas composition in the bench-scale gasifier experiments. An analysis for forward propagation of uncertainties was performed and results show that an increase in steam to oxygen ratio leads to an increase in H2 mole fraction and a decrease in CO mole fraction. These findings are in agreement with the ANOVA analysis performed in the reference experimental study. Another contribution in addition to the UQ analysis is the optimization-based approach to guide to identify next best set of additional experimental samples, should the possibility arise for additional experiments. Hence, the surrogate models constructed as part of the UQ analysis is employed to improve the information gain and make incremental recommendation, should the possibility to add more experiments arise.

In the second step, series of simulations were carried out with the open-source computational fluid dynamics software MFiX to reproduce the experimental conditions, where three operating factors, i.e., coal flow rate, coal particle diameter, and steam-to-oxygen ratio, were systematically varied to understand their effect on the syngas composition. Bayesian UQ analysis was performed on the numerical results. As part of Bayesian UQ analysis, a global sensitivity analysis was performed based on the simulation results, which shows that the predicted syngas composition is strongly affected not only by the steam-to-oxygen ratio (which was observed in experiments as well) but also by variation in the coal flow rate and particle diameter (which was not observed in experiments). The carbon monoxide mole fraction is underpredicted at lower steam-to-oxygen ratios and overpredicted at higher steam-to-oxygen ratios. The opposite trend is observed for the carbon dioxide mole fraction. These discrepancies are attributed to either excessive segregation of the phases that leads to the fuel-rich or -lean regions or alternatively the selection of reaction models, where different reaction models and kinetics can lead to different syngas compositions throughout the gasifier.

To improve quality of numerical models used, the effect that uncertainties in reaction models for gasification, char oxidation, carbon monoxide oxidation, and water gas shift will have on the syngas composition at different grid resolution, along with bed temperature were investigated. The global sensitivity analysis showed that among various reaction models employed for water gas shift, gasification, char oxidation, the choice of reaction model for water gas shift has the greatest influence on syngas composition, with gasification reaction model being second. Syngas composition also shows a small sensitivity to temperature of the bed. The hydrodynamic behavior of the bed did not change beyond grid spacing of 18 times the particle diameter. However, the syngas concentration continued to be affected by the grid resolution as low as 9

times the particle diameter. This is due to a better resolution of the phasic interface between the gases and solid that leads to stronger heterogeneous reactions.

This report is a compilation of three manuscripts published in peer-reviewed journals for the series of studies mentioned above.

1. INTRODUCTION

The development of advanced clean technologies to enable the continued use of abundant and affordable fossil energy such as coal resources across the United States for power generation is one of the critical missions of the National Energy Technology Laboratory (NETL) of the U.S. Department of Energy [1]. One such technology is carbon feedstock gasification, which promises to couple high efficiency, with low pollutant for power generation and chemical production. An integrated approach that combines theory, computational modeling, experimentation, and industrial feedback to develop physics-based methods, models, and tools to support the development and deployment of advanced gasification-based reactors and systems is critical for the development of next generation clean energy technologies. Hence, objective assessment of the reliability and predictive capability of computational modeling tools such as computational fluid dynamics (CFD), which can simulate complex flows in coal gasifiers will play an important role for reducing design cycle and faster time-to market.

The need for this objective assessment of prediction credibility is even greater in multiphase gas-solid flow CFD modeling, since the solid phase flow field can fluctuate both spatially and temporally with amplitudes of the order of the mean flow [2]. To address this need, uncertainty quantification (UQ) techniques and analysis have been employed in the recent years by many researchers. Hence, uncertainty quantification methods are being used at NETL in order to assess diverse sources of uncertainties encountered in reacting multiphase flow modeling of advanced gasifiers. This was achieved by first exploring the applicability of uncertainty quantification methods for multiphase flows to an existing experimental dataset. For this purpose, the experiment results from a bench-scale fluidized bed gasifier obtained from Karimipour et al. [3] was used. Bayesian UQ methods were used to better understand the governing physics and sensitivities of the operating conditions varied during experiments on the quantities of interest such as the syngas composition obtained from the author [4].

Once the applicability of Bayesian UQ methods to experimental data from the bench scale fluidized bed gasifier was established, the UQ methodology was applied to simulation results of the same fluidized bed gasifier conducted with CFD open source software MFiX [5]. Aside from uncertainties associated with numerical approximations that are inherently present in any simulation, multiphase flow modelers have to account for additional uncertainties due to the various closure models that are based on empirical observation and constitutive relationships, (Lane et al. [6]). Additionally, accounting for the heat and mass transfer between the gaseous and solid phases that takes place in reacting flows further complicates simulations by introducing more sources of error and uncertainty with chemical reaction time scales that can be a few orders of magnitude smaller than the hydrodynamic time scale of the flow. In the current study the effect that reaction models for gasification, char oxidation, carbon monoxide oxidation and water gas shift will have on the syngas composition at different grid resolution, along with bed temperature, which affects the reactions have been also studied.

2. BENCH SCALE FLUIDIZED BED GASIFIER EXPERIMENT

The experimental study performed by Karimipour et al. [3] for a bench-scale fluidized bed gasifier was selected for exploring the applicability of various uncertainty quantification methods in reacting multiphase flows. Karimipour et al. [3] performed series of gasification experiments to characterize the effect of coal feed rate (will be referred as Factor #1, which was varied between 0.036 g/s and 0.063 g/s), coal particle size (Factor #2 varied between 70 μm and 500 μm) and steam to oxygen ratio (Factor #3 varied between 0.5 and 1.0) on the quality of syngas generated. These three operating factors were identified as the most important parameters and a Central Composite Design (CCD) based sampling methodology was employed to vary them at three distinct levels in a systematic way. The relationship between operating variables and the quantities of interest in the experiment were approximated with Response Surface Methodology (RSM). This experimental study was unique in a way that extensive experimental data was generated as the identified parameters were varied in a systematic manner by employing statistical design of experiments methods to construct a response surface, which was then used to assess the effect of these operating conditions on the response parameters (a.k.a. quantities of interest) such as H_2/CO ratio. However, the original study was limited to a basic analysis of variance (ANOVA) investigation of the experimental results. In our study, an uncertainty quantification analysis was performed with the experimental data obtained from [3] prior to our CFD simulation campaign for the same configuration and the follow-up UQ analysis [7]. For example, forward propagation of uncertainties was performed with the experimental data acquired to better quantify the potential effect of uncertainties in the operating factors. Also in the original published study, the response variables or quantities of interest were limited to derived quantities such as carbon conversion, gasification efficiency or ratio of select species mass fractions. To avoid performing UQ analysis with the derived quantities, all analysis was performed with species mole fractions (e.g., CH_4, CO etc.). **Error! Reference source not found.** shows the mole fraction of key components of the syngas measured by Karimipour et al. [4].

Karimipour et al. [3] used the CCD sampling method, depicted in Figure 1, to come up with 15 distinct experimental conditions by varying factors 1 to 3 at the same time in a systematic way to capture their effect on the response variables. One of the experimental conditions, was replicated 6 times. Although statistical design of experiments techniques strongly recommends randomization and replication of all samples to increase the confidence in experimental measurements, the physical experiments were not conducted completely following these principles. The replication runs, which were performed for the center point were the experiments conducted with coal flow rate = 0.0495 g/s, coal particle size = 285 μm, steam to oxygen ratio = 0.75. In addition to the experiments performed based on CCD based grid sampling, 4 additional experiments were conducted for validation purposes where the steam to oxygen ratio was kept at 0.75 but other two factors were varied at the upper and lower limits. In our study, the available replications of the same experimental condition were useful in assessing and estimating the experimental errors, and the additional 4 experiments were used in assessing the quality of the

surrogate model constructed with Gaussian Process model approach, which is discussed in the following sections.

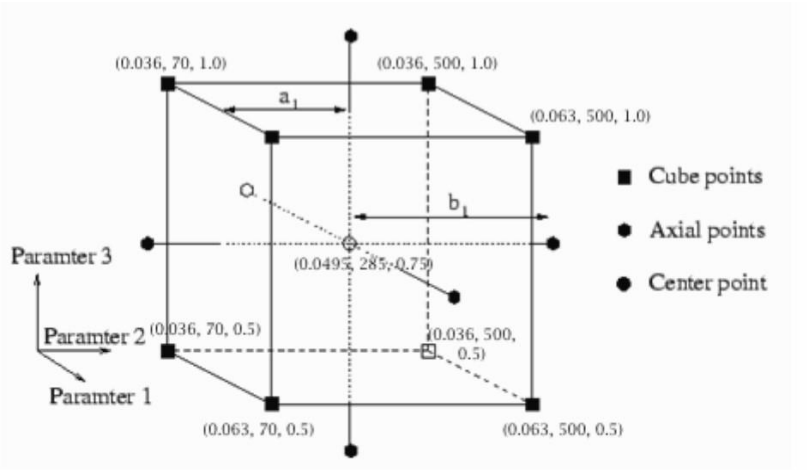

Figure 1 Central Composite Design (CCD) illustration [8]

	Uncertain Input Parameters/Factors			**Secondary Quantities of Interest (Karimipour** [4]**)**				
Actual Experiment Run Order	Factor 1	Factor 2	Factor 3	Response 6	Response 7	Response 8	Response 9	Response 10
	Coal Flow Rate (g/s)	Particle Size (μm)	H2O/O2 Ratio in syngas	CH4 mole fraction	CO mole fraction	CO2 mole fraction	H2 mole fraction	N2 mole fraction
1	0.063	**70**	0.5	0.0074	0.1427	0.1306	0.1149	0.5793
2	0.063	**70**	1	0.0073	0.1115	0.1562	0.1393	0.5590
3	0.0495	**70**	0.75	0.0076	0.1296	0.1431	0.1353	0.5576
4	0.036	**70**	0.5	0.0081	0.1500	0.1256	0.1218	0.5683
5	0.036	**70**	1	0.0078	0.1215	0.1491	0.1512	0.5427
6	0.063	**285**	0.75	0.0078	0.1316	0.1394	0.1349	0.5592
7	0.0495	**285**	0.5	0.0077	0.1448	0.1300	0.1172	0.5752
8	0.0495	**285**	0.75	0.0080	0.1357	0.1382	0.1349	0.5562
9	0.0495	**285**	0.75	0.0078	0.1357	0.1376	0.1359	0.5559
10	0.0495	**285**	0.75	0.0079	0.1333	0.1396	0.1330	0.5597
11	0.0495	**285**	0.75	0.0084	0.1414	0.1354	0.1426	0.5448
12	0.0495	**285**	0.75	0.0080	0.1352	0.1378	0.1371	0.5552
13	0.0495	**285**	0.75	0.0079	0.1345	0.1383	0.1344	0.5586
14	0.0495	**285**	1	0.0074	0.1143	0.1534	0.1395	0.5588
15	0.036	**285**	0.75	0.0077	0.1322	0.1393	0.1352	0.5587
16	0.063	**500**	0.5	0.0079	0.1395	0.1330	0.1168	0.5781
17	0.063	**500**	1	0.0076	0.1119	0.1557	0.1419	0.5556
18	0.0495	**500**	0.75	0.0079	0.1272	0.1441	0.1299	0.5660
19	0.036	**500**	0.5	0.0080	0.1500	0.1262	0.1143	0.5767
20	0.036	**500**	1	0.0080	0.1243	0.1487	0.1502	0.5419

Table 1 Tabulated data for input and secondary quantities of interest (response) from experiments [4]

3. BAYESIAN UNCERTAINTY QUANTIFICATION ANALYSIS METHOD

General Electric Bayesian Hybrid Modeling (GEBHM), first proposed by Kennedy and O'Hagan [9] and jointly developed by Los Alamos National Laboratory (LANL) and General Electric (GE), is a generalized technique for probabilistic calibration of simulation models under uncertain conditions. Conceptually, the principle of Bayesian Hybrid Modeling (BHM) can be expressed as,

$$\boldsymbol{y(x_i)} \pm \boldsymbol{\epsilon(x_i)} = \boldsymbol{\eta(\theta, x_i)} + \boldsymbol{\delta(x_i)}; \quad \boldsymbol{i = 1 \ldots n} \qquad \textbf{(1)}$$

where, n is the number of experimental observations, $y(x)$ denote the observation from the experiments, $\eta\ (x_i,\theta)$ denote the high fidelity simulator (such as the CFD model), with x being the controllable design parameters (with variability), and $\hat{\theta}$ being the true values of the additional un-observable model parameters (referred to as calibration or tuning parameters), $\delta(x)$ is the discrepancy between the calibrated simulator η and the experimental observation, and are the well-characterized observation errors (an input to the Bayesian framework) as shown in Figure 2. GE has co-developed the GEBHM framework for the Bayesian calibration of large-scale (100+ parameters) industrial applications. The unique feature of this technique is the explicit formulation where the high-fidelity physics model is considered to be potentially deficient and thus the discrepancy model is included during the calibration phase. This means that the calibration of the model parameters and the computation of the discrepancy occur simultaneously. This prevents the model from being over-tuned because the Bayesian framework favors solutions where both the calibration parameters and the discrepancy term are highly likely and thus automatically filters one-off over-tuned results. This ensures that the physics model is predictive over the entire design space.

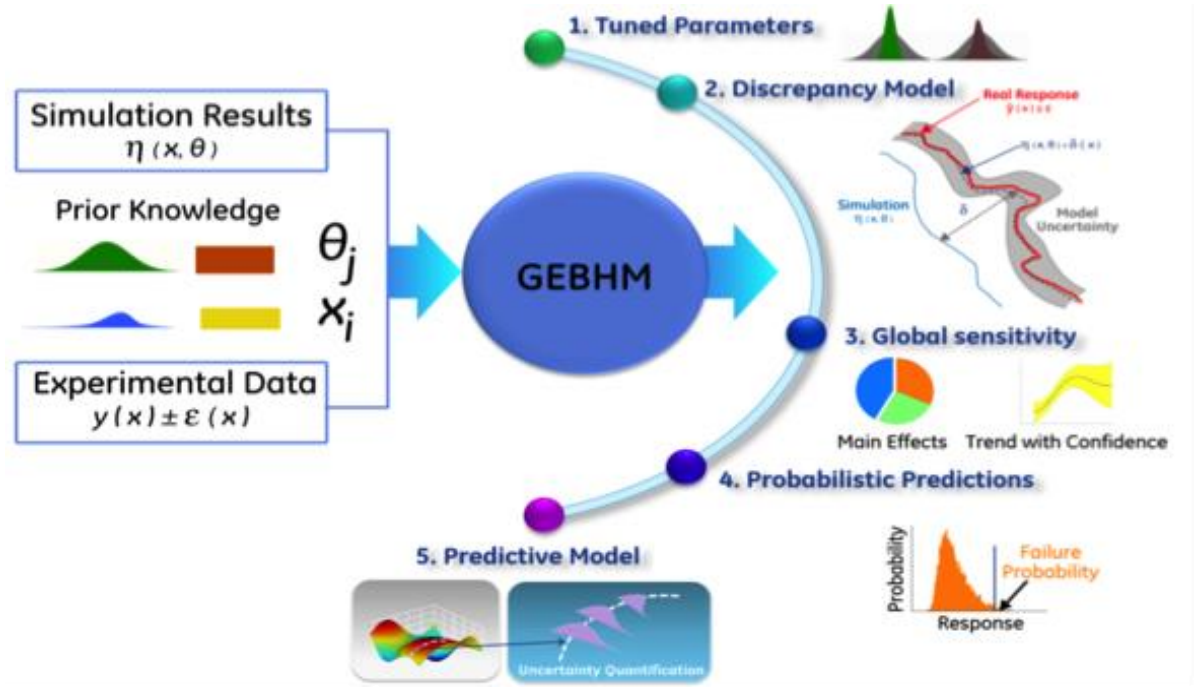

Figure 2 Bayesian Hybrid Method illustration

These techniques have been successfully applied within GE for calibrating complex nonlinear systems under uncertain conditions such as engine system-level thermal model calibration and validation (with more than 100 parameters involved), global sensitivity and optimization for design and improved model predictive capability for combustion dynamics, thermo-mechanical design, alloy design, etc. ([10], [11]).

In general, the high fidelity simulator results are not always available at the experimental setting, but rather on a set of m design and calibration parameter combinations $\eta(x_j,\theta_j)$ for $j = 1,2,\ldots m$. The optimal simulations are usually chosen based on an experimental design procedure. As proposed by Kennedy & O'Hagan [20], and as described by Higdon et al. [12], the simulator output and model discrepancy are modeled as Gaussian Processes (GP). The GP models become the priors for the simulator outputs, discrepancy and outputs y, which can be expressed in the following way:

$$\hat{\boldsymbol{y}}(\boldsymbol{x_i}) \pm \boldsymbol{\epsilon}(\boldsymbol{x_i}) = \boldsymbol{\eta}(\boldsymbol{\theta}, \boldsymbol{x_i}) + \boldsymbol{\delta}(\boldsymbol{x_i}); \quad \boldsymbol{i} = \boldsymbol{1} \ldots \boldsymbol{n} \qquad \textbf{(2)}$$

The simulator outputs at m design locations (x_j,θ_j) are known. The simulator η is approximated as a GP model with a zero mean, and covariance matrix given by a block diagonal matrix (each block of size $m \times m$). The non-zero terms of the covariance matrix are given below.

$$\sum_{ij}^{\eta k} = \frac{1}{\lambda_{\eta z}} \exp\left(\beta_{\eta k} |X_i - X_j|^2\right) + I \frac{1}{\lambda_{\eta s}} \quad (3)$$

for i,j=1,...,m and k=1,...,N.

where the X is the combined vector of design and calibration parameters ($X = (x,\theta)$) used to generate the simulation outputs, the parameters $\lambda_{\eta z}$ and λ_{etas} characterize the marginal data variance captured by the model and by the residuals, respectively, $\beta_{\eta k}$ characterizes the strength of dependence of k^{th} output on the design (x) and calibration (θ) parameters. The exponent 2 ensures the GP model is smooth, and is infinitely differentiable. The experimental output y is also modeled through a similar GP.

The posterior distributions of the calibration parameters and the hyperparameters of the GP models are evaluated using the Markov Chain Monte Carlo (MCMC) approach. A modified version of Metropolis-Hastings algorithm was used with univariate proposal distributions for the MCMC posterior updates. The initial values of the covariance matrices are updated with current realizations of the hyperparameters at every MCMC step. Realizations from the posterior distributions of the hyperparameters are produced using MCMC. This customized version of MCMC was specifically modified to enable parallel execution for optimized performance, which makes GEBHM approach unique as compared to other available Bayesian codes [11]. In the first part of the study global sensitivity analysis, and forward propagation of uncertainties are demonstrated using the GEBHM by utilizing the experimental data only. Hence, for the purposes of the initial part of the study presented no CFD simulation data was employed with the GEBHM analysis. A brief summary of the theory behind computing global sensitivity analysis is provided below section to provide insight for the reader on the methodology employed.

3.1 GLOBAL SENSITIVITY ANALYSIS

One of the fundamental analysis employed as part of the uncertainty quantification assessment is the global sensitivity analysis. It aims to answer the question of which input factors have the most influence on the variability observed for the quantities of interest for a given parameter space and accordingly limited resources can be allocated to reduce the uncertainty in those input factors. In other words, it attempts to answer the question of which set of input factor(s) drive the variability observed in the quantities of interest and to what extent in the entire design space. In traditional sensitivity analysis, the gradients at a fixed point in the design space (typically at the mean) are used to assess sensitivity of individual factors. In non-linear systems with several parameters, this provides a very limited view of sensitivity. Hence, global sensitivity offers a holistic view of sensitivity in the full design space and thus provides a complete coverage for design. After the construction of the GPM based emulator from the available experimental data, global sensitivity analysis was performed utilizing the GEBHM framework.

Let us consider a response y that is a function of n variables:

$$y = g(x_1, x_2, \dots, x_n), \quad where \ x_i \in [0,1] \quad (4)$$

Variance based global sensitivity analysis use Sobol' indices to denote relative significance of variables. The Sobol' decomposition of y is given by:

$$\boldsymbol{y = f_0 + \sum_{i=1}^{n} f_i\,(x_i) + \sum_{1\le i\le j\le n} f_{ij}(x_i, x_j) + \cdots f_{1,2,\ldots,n}(x_1, x_2, \ldots, x_n)} \quad \textbf{(5)}$$

The effect functions f is defined as shown below.

$$\boldsymbol{f_0 = Mean\,[y] = \int g(x)dx} \quad \textbf{(6)}$$

The main effect functions are defined as the integrated effect of all inputs except x_i.

$$\boldsymbol{f_x(x_i) = \int g(x)_{\sim i}\, dx - f_0} \quad \textbf{(7)}$$

Two-way interaction effect functions are computed by integrating $g(x)$ with all inputs except the inputs x_i and x_j and subtract the main effect functions of x_i and x_j and the mean of $g(x)$. Higher order interaction effects can be written in a similar fashion. Using the above main and interaction effect functions we can compute the Sobol' indices. Let D denote the variance of the true function $g(x)$.

$$\boldsymbol{D = Var\,[g(x)] = \int g^2(x) - f_0^2} \quad \textbf{(8)}$$

By integrating the square of Equation 1 and invoking the orthogonality property, we can write:

$$\boldsymbol{D = \sum_{i=1}^{n} D_i + \sum_{1\le i\le j\le n} D_{ij} + \cdots + D_{1,2,\ldots,n}} \quad \textbf{(9)}$$

Where $D_i = \int f_i^2\,(x_i)\,dx_i$

Sobol' indices are then defined as below:

Main effects:

$$\boldsymbol{S_i = \frac{D_i}{D}} \quad \textbf{(10)}$$

Two-way interaction effects:

$$\boldsymbol{S_i = \frac{D_{ij}}{D}} \quad \textbf{(11)}$$

All the Sobol' indices sum to 1, i.e.,

$$\boldsymbol{\sum_{i=1}^{n} S_i + \sum_{ij} S_{ij} + \cdots + S_{1,2,\ldots,n} = 1} \quad \textbf{(12)}$$

Each Sobol' index is a sensitivity measure describing which amount of the total variance is due to the uncertainties in the set of input parameters. The first order indices S_i give the influence of each parameter taken alone whereas the higher order indices account for possible mixed influence of various parameters. The Sobol' indices are known to be good descriptors of the sensitivity of the model to its input parameters, since they do not suppose any kind of linearity or monotonicity in the model.

4. BAYESIAN UNCERTAINTY QUANTIFICATION ANALYSIS OF EXPERIMENTAL DATA

The non-intrusive Bayesian uncertainty quantification method introduced in section 3 was used to analyze the results obtained from experiments before proceeding with the simulations. The typical approach involves the following steps:

1. Identify the set of operating factors or input parameters as uncertain parameters, and quantities of interest (QoI) variables (i.e., response parameters)
2. Using statistical design of experiments principles based sampling techniques, design an experiment test matrix to carry out the physical experiments or computational simulations
3. Create surrogate models for the QoIs based on the data generated from step (2) if the experiments or computational models are expensive to run
4. Perform global sensitivity analysis to quantify, which operating factor has the most influence in the variability observed for QoIs
5. Conduct Monte Carlo simulations for forward propagation of input uncertainties by using random drawings from the probability density functions (PDF) that characterize the input uncertainties, and function evaluations of the surrogate models to obtain histograms for QoIs.

Steps (1) and (2) have already been determined by the experimental work of Karimipour et al. [3]. The next step is the construction of the appropriate surrogate model. The original study ([3]) relied on a simple polynomial regression based response surface, which is typically used in traditional physical design of experiments setup rather than UQ analysis. The QoIs were mostly derived QoIs (e.g., gasification efficiency). In the current study, the additional quantities of interest based on mole fractions such as CO, H_2 and CO_2 mole fractions are also included. These QoIs are directly obtained from the author of original study [4].

The tabulated experimental conditions and measured quantities of interest variables for 20 physical experiments in [3] were used as input for the GEBHM analysis. The first step in the GEBHM framework is to construct a Gaussian Process Model (GPM) based surrogate model (a.k.a. the emulator) of the responses, which is capable of modeling nonlinear responses accurately as compared to the simple polynomial regression based response surfaces generated in the original study [3]. However, GPM based emulators, which were used in our study, possess a unique feature that is not available in regression based response surface methods, i.e., an assessment of the uncertainty of the emulator constructed without any additional computation. This is shown in the color contours of the 3D surface plots for the emulators constructed for CO, H_2 and CO_2 mole fractions as shown in Figure 3 through Figure 5. The color legend shows the uncertainty in the emulator based on the given set of experimental data points. A practical way to interpret the uncertainty pattern observed in the color contours is based on the fact that the CCD sampling design contains data points on the corners of a cube and faces, the uncertainty is lower around these sampling points and increases as one gets further away, which is shown with the yellow color range.

In these surface plots, the steam to oxygen ratio and coal particle size are shown in x and y axis respectively for each quantity of interest. The third operating factor, coal flow rate was kept at nominal setting corresponding to the mid-point value in the plots for evaluation purposes. It is

noted that in the original study by Karimipour et al., similar plots for the quantities of interest were also generated based on the polynomial regression based response surface constructed but they were primarily for the derived quantities of interest such as gasification efficiency excluding the two ratios, i.e., H_2/CO and CH_4/H_2. In the current study, as discussed earlier, standalone mole fractions for the species of interest were considered and used throughout the analysis. Figure 6 was provided for qualitative comparison of GPM based emulator with respect to polynomial regression based response surface for the same quantity of interest, i.e., H_2/CO. Similar conclusions can be derived from the GPM based emulators constructed, i.e., as shown in Figure 3 through Figure 5 the production of syngas species CO, H_2 and CO_2 increases as the ratio of steam to O_2 increases with coal particle diameters having no effect on variability of syngas composition. This indicates that the fluidization behavior is not effected by particle size range used in the experiment. The remainder UQ analysis such as global sensitivity analysis was based on the GPM based emulators constructed from the experimental dataset (Figure 3 through Figure 5).

4.1 ASSESSMENT OF SURROGATE MODEL QUALITY

Assessment of the quality of the emulator is a key step in non-intrusive UQ analysis process as the rest of the UQ analysis heavily relies on the quality of the emulator constructed in lieu of the CFD simulations. Figure 7 shows a comparison of the actual and predicted values from the GEBHM emulator for each of the responses. Ideally, the model predictions should be as close as possible to the experimentally observed values, i.e., have points along the diagonal in the plot. Any deviations from the diagonal is related to the model approximation and experimental errors. As shown in Figure 7, the GEBHM surrogate models predict all quantities of interest accurately. In the case of the five repeats in the experimental data for center point conditions, the emulator predicts the mean of the repeated experimental points accurately and the uncertainty of the prediction reflects the uncertainty introduced by the variation in the repeated results.

Another approach to assess the quality of the surrogate model was predicting the validation runs in the experiment with the surrogate model. For this purpose, the four additional experiments listed in [3] under validation runs were predicted with the Gaussian Process Model based surrogate model. The results of the discrepancy are shown in Table 2. Comparison between actual experiment data for H_2/CO and predictions from emulator, shows a maximum discrepancy of 4.5%. This is particularly good given that the original dataset was not a space-filling design of experiments such as Latin hypercube based sampling. GP models prefer the input data to be distributed throughout the entire design space rather than be sampled with traditional Central Composite Design based grid sampling. In spite of this limitation, it can be seen that the model captures the main effects well as seen by the good predictions. The lack of space filling distributed points in the input space might restrict the model to main effects and minimal interactions.

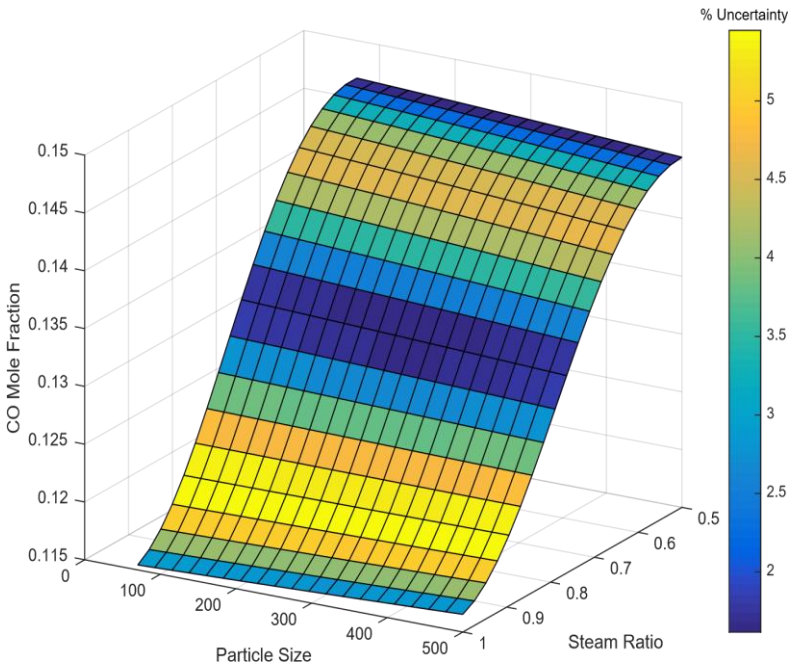

Figure 3 CO surrogate model (emulator) behavior. Color represents % uncertainty in the surrogate model primarily due to sampling method and samples

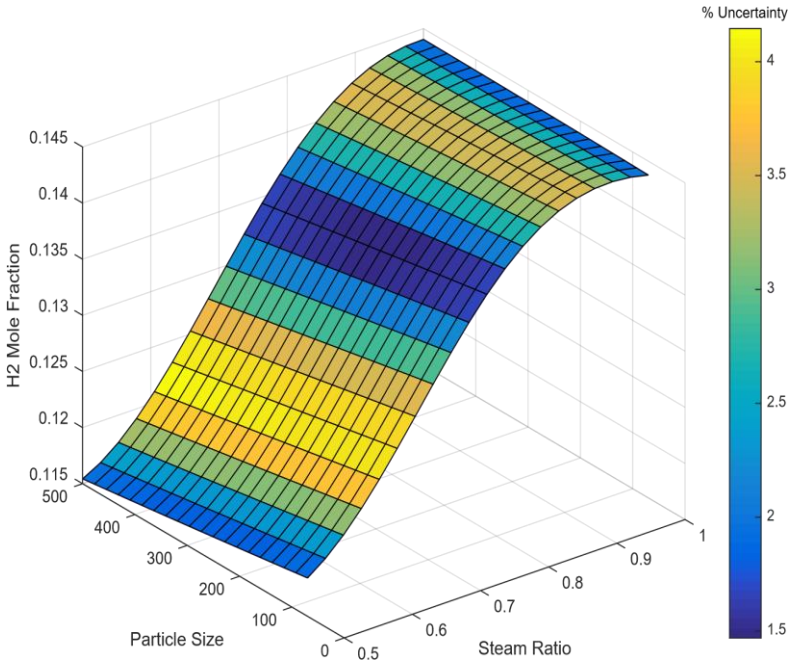

Figure 4 H_2 surrogate model (emulator). Color represents % uncertainty in the surrogate model primarily due to sampling method and samples

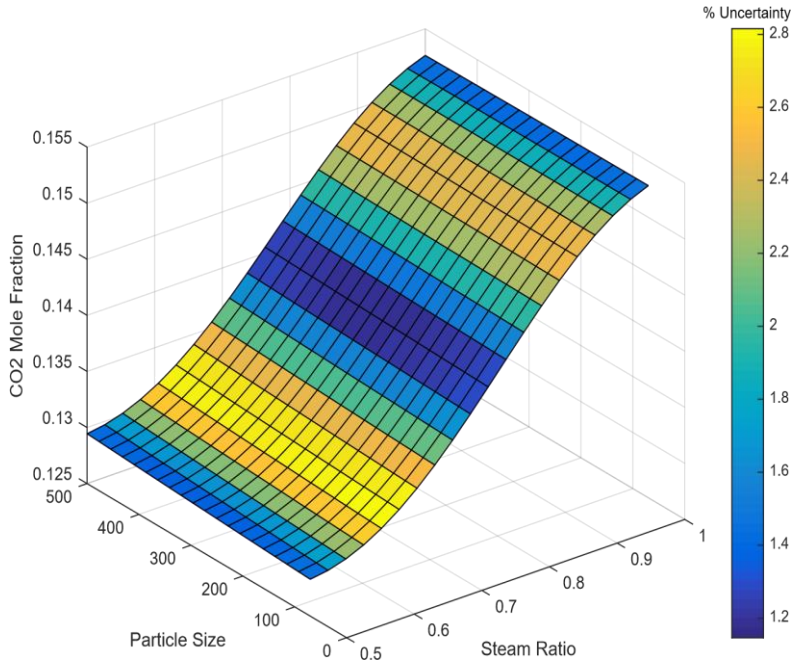

Figure 5 CO_2 surrogate model (emulator). Color represents % uncertainty in the surrogate model primarily due to sampling method and samples

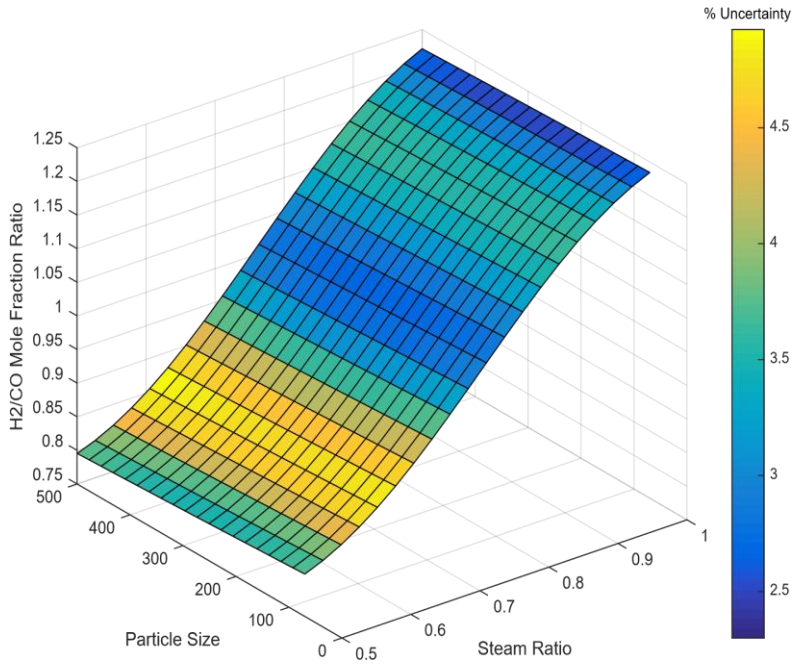

Figure 6 Surface plot showing the surrogate model (emulator). Color represents % uncertainty in the surrogate model primarily due to sampling method and samples

Coal Flow Rate (g/s)	Particle Size (μm)	Steam/O_2	H_2/CO experiments	H_2/CO emulator	Discrepancy
0.063	500	0.75	1.065	1.0173	-4.5%
0.036	500	0.75	1.013	1.0059	-0.7%
0.63	70	0.75	1.009	1.0256	1.6%
0.036	70	0.75	1.003	1.0333	3.0%

Table 2 Comparison of Additional Validation Runs with respect to Surrogate Model (emulator) Predictions

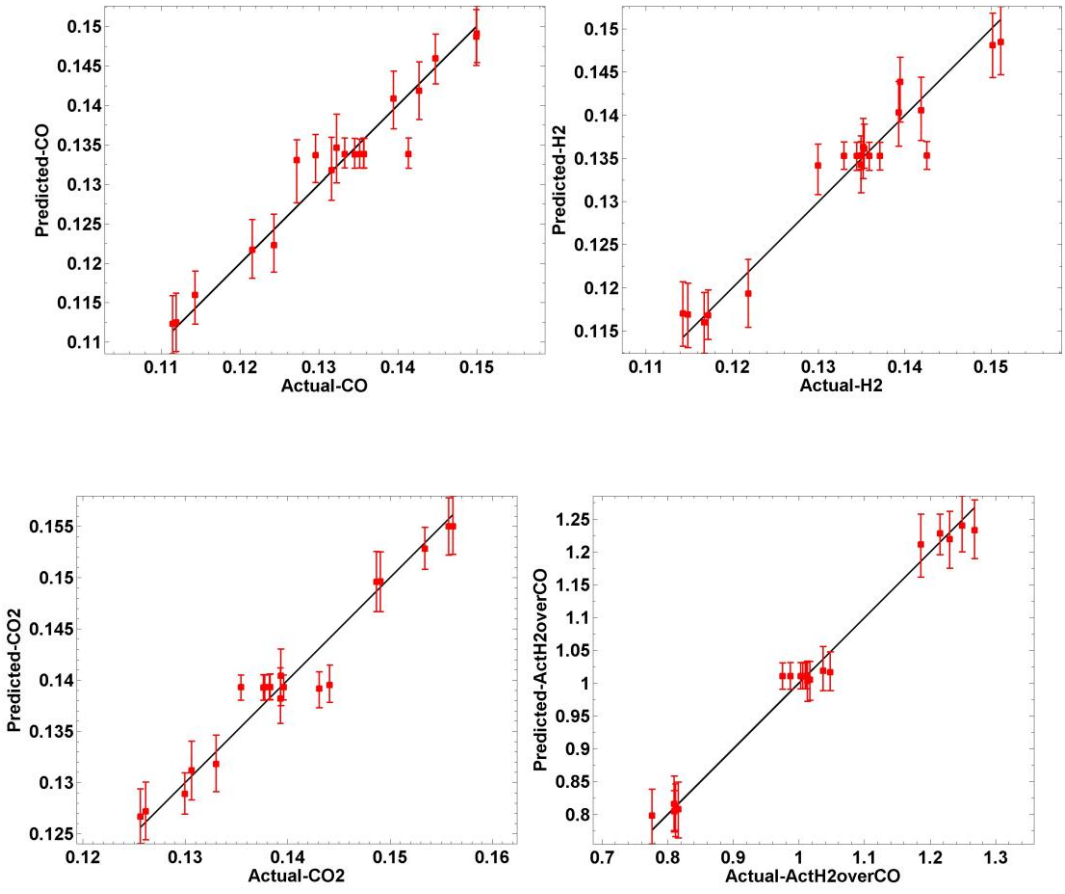

Figure 7 GEBHM surrogate model (emulator) quality for each QoI

4.2 GLOBAL SENSITIVITY ANALYSIS

As part of the uncertainty quantification assessment, a global sensitivity analysis, which aims to understand the relative effect of input parameters on the variability observed in the quantities of interest was performed with GEBHM. A brief summary of the theory behind computing global sensitivity analysis is provided in section 3.1, the results of the sensitivity analysis when applied to the available experimental data is presented in this section.

Table 3 shows the global sensitivity analysis results for the experimental data. The results show that the sensitivity is primarily due to main factors (i.e., three operating factors varied during the experiments) rather than their interactions with each other being more influential on the quantities of interest. There may be governing physics where interaction of certain main factors plays a key role in the variability observed for quantities of interest. The global sensitivity analysis can isolate the contribution from main factors versus interaction of the main effect factors (i.e., coal flow rate and steam to oxygen ratio at the same time). Among the three main factors considered in the experiment, steam to oxygen ratio appears to have the most pronounced effect on CO, H_2 and CO_2 mole fractions as shown in the bottom row of Table 3 in tabulated format. For example, the variability observed in CO mole fraction at the monitoring location of the gasifier is primarily (97%) due to steam to oxygen ratio and 1.6% due to coal flow rate. Among the interaction of main effects, only the interaction of coal flow rate with steam to oxygen ratio appears to be above 1 % (as shown in the off-diagonal cells), which is insignificant compared to the effect of steam to oxygen ratio standalone. Similar situation is observed with the remaining QoIs. This type of insight is quite critical in understanding the effect of uncertainty in certain input parameters on the quantities of interest and support decision making such as in allocating more resources for focused experiments to reduce the uncertainty in these input parameters.

It is worth noting that the results of the sensitivity analysis are skewed by the sampling method that was employed for varying the inputs. By design, Central Composite Design sampling prevents exploring higher order interactions. Thus, the lack of interactions seen in the experimental data should not be taken as evidence that interaction effects are minimal. Interrogating the system with space filling designs such as Optimal Latin Hypercube (OLH) sampling is required to accurately quantify interaction effects. We investigated this as part of a study which is carried out through computational fluid dynamics simulations of the same fluidized bed gasifier [13].

The variance in global sensitivity for each QoI is shown in Figure 8. These plots show the overall sensitivity of each factor or operating variable to the corresponding quantity of interest. The median of the sensitivity is shown as a red line in the box plot. A sensitivity value close to zero indicates low sensitivity and close to one indicates very high sensitivity [14]. For every QoI, the steam to oxygen ratio is identified as the most sensitive parameter. However, since the variance in sensitivity for this parameter ranges from 0 to 1, the sensitivity varies significantly depending on the location in the design space, i.e., depending on where the other two variables are set, the steam ratio could be very sensitive or completely insensitive. Hence, although coal flow rate and particle size don’t effect syngas composition directly, they are still very important since they influence steam to oxygen ratio, which is the most sensitive parameter. Application of Bayesian

UQ analysis for the experimental data clearly shows that steam to oxygen ratio has the most pronounced effect on all quantities of interest under consideration.

4.3 FORWARD UNCERTAINTY PROPAGATION

The forward propagation of uncertainties analyzes the effect of input variables' uncertainty on the quantities of interest parameters. The GEBHM models were used for forward uncertainty propagation of input variables for various different cases, which are presented in this section and summarized in Table 4. It is noteworthy that the objective of this section is to illustrate the utility of forward uncertainty propagation for performance analysis of a gasifier. For that reason, the parameters in Table 4, along with their distribution are meant to be examples rather than what has been observed in the bench scale gasifier under study. For this purpose, each factor was either kept constant at a setting or considered to be uncertain with a probability density function (PDF) assigned to it. For example, in case # 2 the coal particle size was considered to be uncertain and characterized with a Gaussian probability density function (PDF) based distribution, which had a mean of 285 microns and standard deviation of 28.5 microns (denoted as $\sim N(285,28.5)$).

Coal particle size was chosen as the uncertain operating parameter for forward propagation due to the fact that coal diameter variability in batches of coal is one of the common observations in commercial scale operations. The fundamental idea is to identify a set of input or operating parameters to be considered as uncertain and characterize the associated uncertainty through probability density function (PDF) for aleatory uncertainties.

The GPM emulator was used with random samples from the associated PDF to compute the quantities of interest, e.g., species mole fraction CO, H_2 and their ratio each time. A sample size of 10,000 was used to propagate uncertainty through the GEBHM model. Further information on different types of uncertainties and how forward propagation of input parameters can be performed is presented in Roy et al. [15] and Gel et al. [16].

The mean and standard deviation for the histograms of quantities of interest are provided in Table 5. As seen in the Table 5, the sample mean and standard deviation used in each case is listed in a tabulated format, which might be difficult to interpret standalone. Hence, the empirical cumulative density function (eCDF) plot for each QoI and for all UQ cases have been compiled to facilitate easier interpretation of the results obtained and relative comparison through likelihood readings for observation of certain values of the QoIs. Figure 9 through Figure 12 show the eCDF plots where results obtained from cases 1 to 4 are superimposed in the same eCDF plot for each quantity of interest. Similarly, Figure 13 through Figure 16 show the eCDF plots where results obtained from cases 5 to 9.

	Factor 1	Factor 2	Factor 3
	CF	PS	H2O/O2
CF: Coal flow rate (g/s)	1.6%	0.05%	1.1%
PS: Particle size (µm)		0.2%	0.1%
H2O/O2 ratio in syngas			96.9%

% Contribution of variability seen in CO mole fraction

	Factor 1	Factor 2	Factor 3
	CF	PS	H2O/O2
CF: Coal flow rate (g/s)	0.9%	0.32%	1.7%
PS: Particle size (µm)		1.4%	0.4%
H2O/O2 ratio in syngas			95.3%

% Contribution of variability seen in H2 mole fraction

	Factor 1	Factor 2	Factor 3
	CF	PS	H2O/O2
CF: Coal flow rate (g/s)	1.0%	0.01%	0.6%
PS: Particle size (µm)		0.1%	0.1%
H2O/O2 ratio in syngas			98.3%

% Contribution of variability seen in CO2 mole fraction

Table 3 Global Sensitivity of Quantities of Interest (QoI) with respect operating variables.

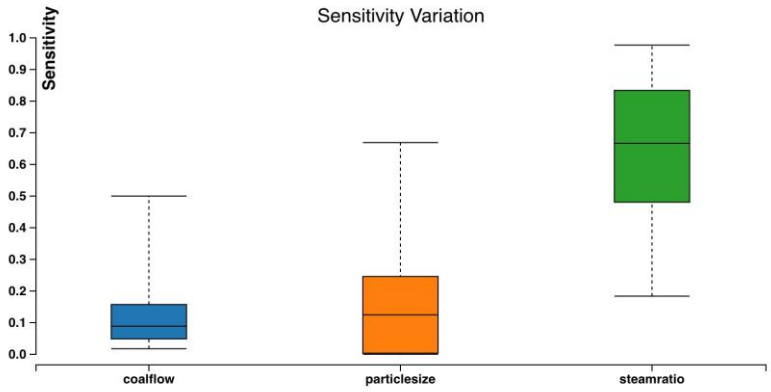

CO

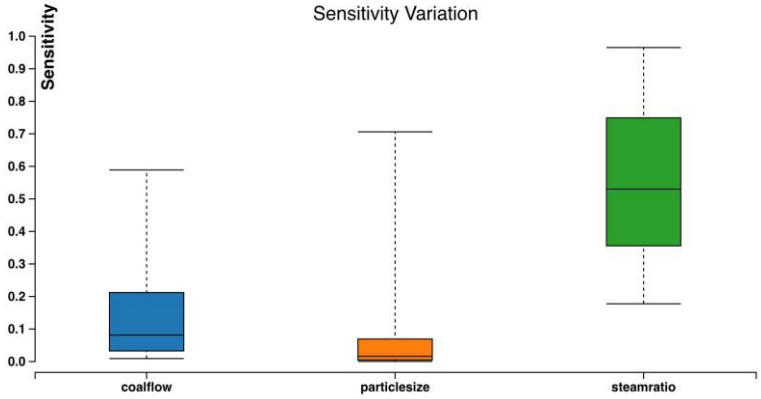

H_2

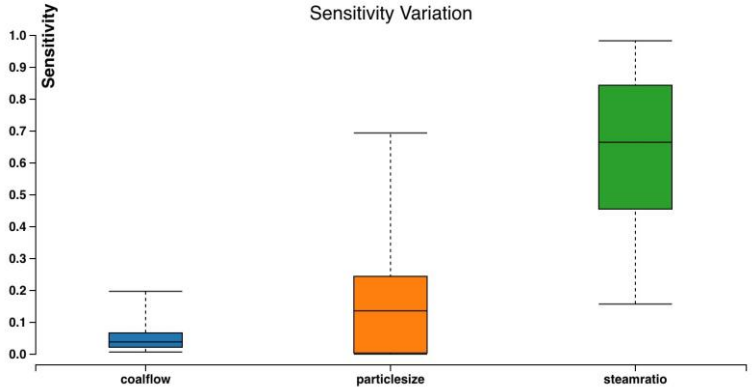

CO_2

Figure 8 Variance of global sensitivity for each QoI.

Case	Coal Flow Rate (g/s)	Coal Particle Size (μm)	Steam/O2 Ratio
1	0.0495	~U(70,500)	0.75
2	0.0495	~N(285,28.5)	0.75
3	0.0495	285	~N(0.75,0.075)
4	0.0495	~N(285,28.5)	~N(0.75,0.075)
5	~N(0.0495,0.00495)	~N(285,28.5)	~N(0.75,0.075)
6	~N(0.0495,0.00495)	~N(285,28.5)	~N(0.5,0.075)
7	~N(0.0495,0.00495)	~N(400,28.5)	~N(0.75,0.075)
8	~N(0.0495,0.00495)	~N(285,28.5)	~N(1.0,0.075)
9	~N(0.063,0.0063)	~N(285,28.5)	~N(0.75,0.075)

Table 4 Input uncertainty forward propagation cases analyzed

	CO		H_2		CO_2		H_2/CO	
Case	μ	σ	μ	σ	μ	σ	μ	σ
1	0.13386	3.84e-4	0.13528	1.09e-3	0.13931	2.04e-4	1.01078	5.99e-3
2	0.13386	8.78e-5	0.13527	2.5e-4	0.13931	4.67e-5	1.01066	1.37e-3
3	0.13349	6.26e-3	0.13455	5.4e-3	0.13948	4.77e-3	1.01047	7.92e-2
4	0.13344	6.14e-3	0.13463	5.3e-3	0.13951	4.68e-3	1.01122	7.7e-2
5	0.13331	6.13e-3	0.13467	5.3e-3	0.13950	4.6e-3	1.01134	7.78e-2
6	0.14464	2.09e-3	0.11817	2.99e-3	0.12983	1.5e-3	0.81633	3.1e-2
7	0.13306	6.e-2	0.13367	5.6e-2	0.13963	4.64e-3	1.00506	7.8e-2
8	0.11723	3.1e-3	0.14302	2.e-3	0.15199	2.3e-3	1.21754	3.6e-2
9	0.13146	6.2e-3	0.13426	5.e-3	0.13997	4.8e-3	1.02465	8.1e-2

Table 5 Summary sample mean (μ) and standard deviation (σ) for quantities of interest for all input uncertainty forward propagation cases

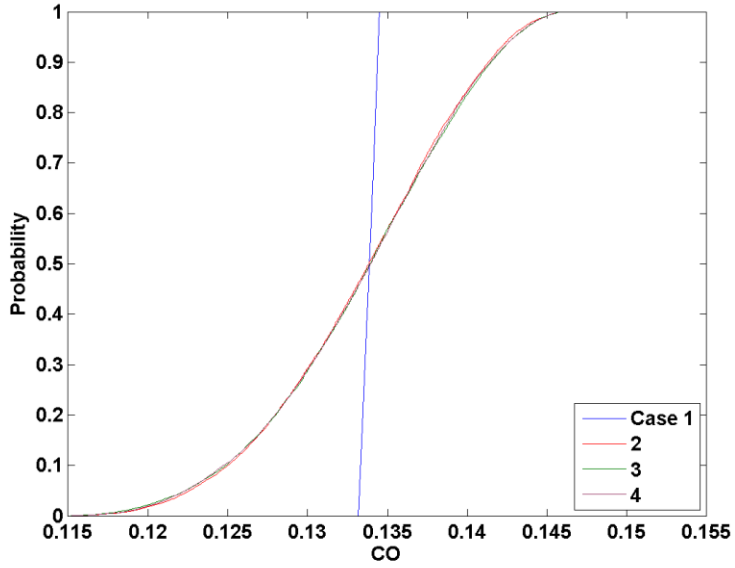

Figure 9 Empirical CDF of posterior distribution of CO mole fraction for UQ cases 1-4

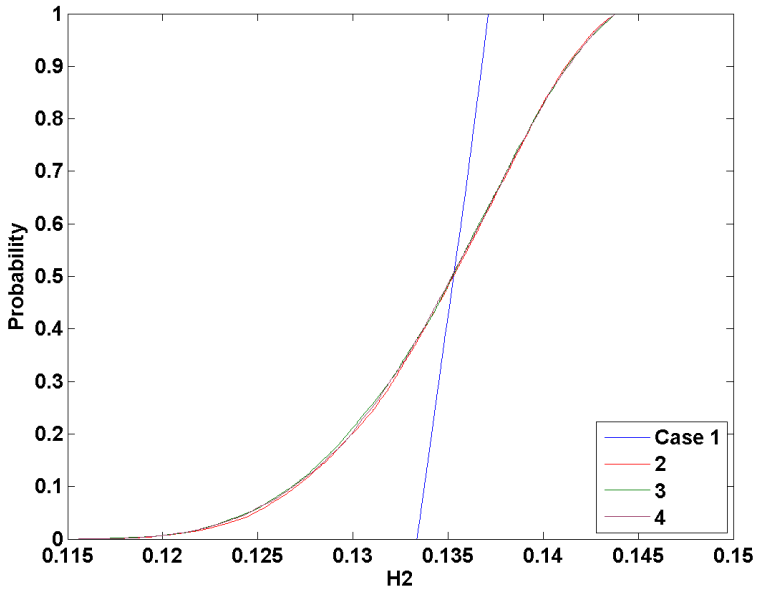

Figure 10 Empirical CDF of posterior distribution of H_2 mole fraction for UQ cases 1-4

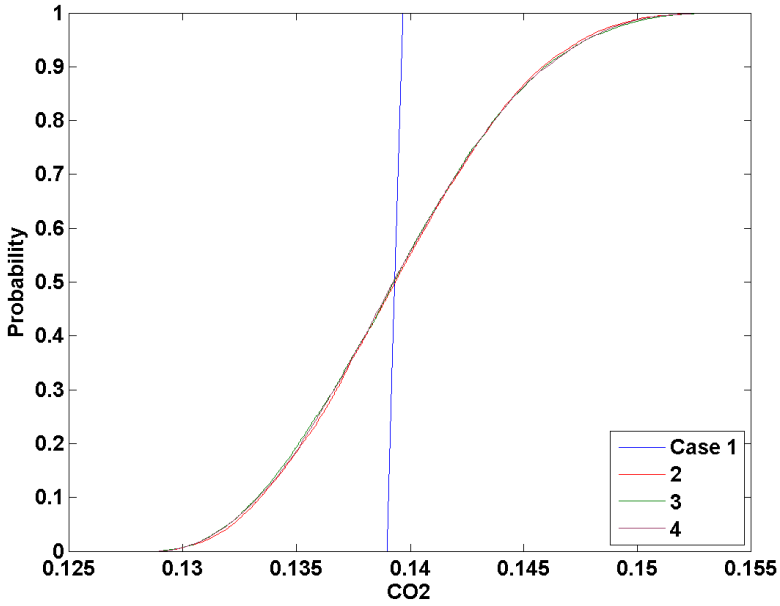

Figure 11 Empirical CDF of posterior distribution of CO_2 mole fraction for UQ cases 1-4

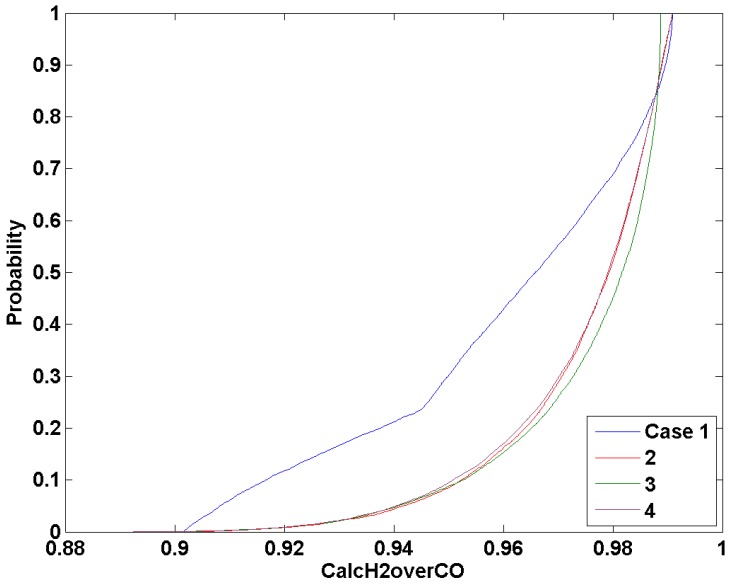

Figure 12 Empirical CDF of posterior distribution of H_2/CO for UQ cases 1-4

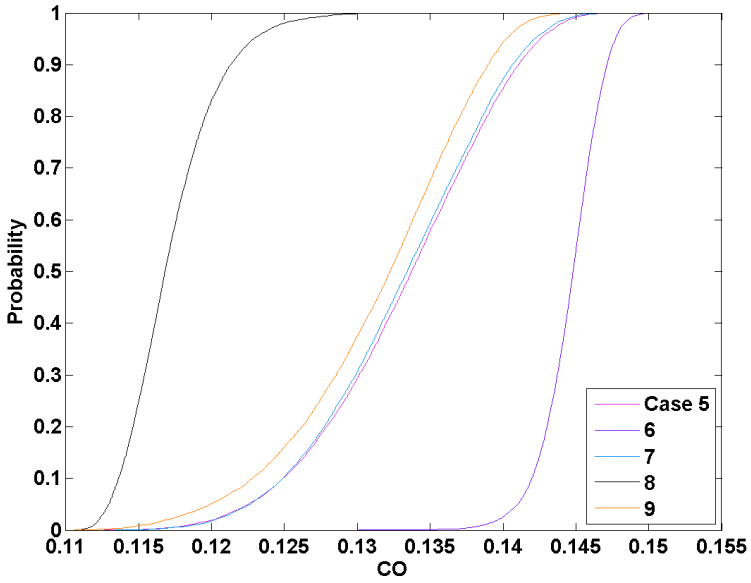

Figure 13 Empirical CDF of posterior distribution of CO mole fraction for UQ cases 5-9

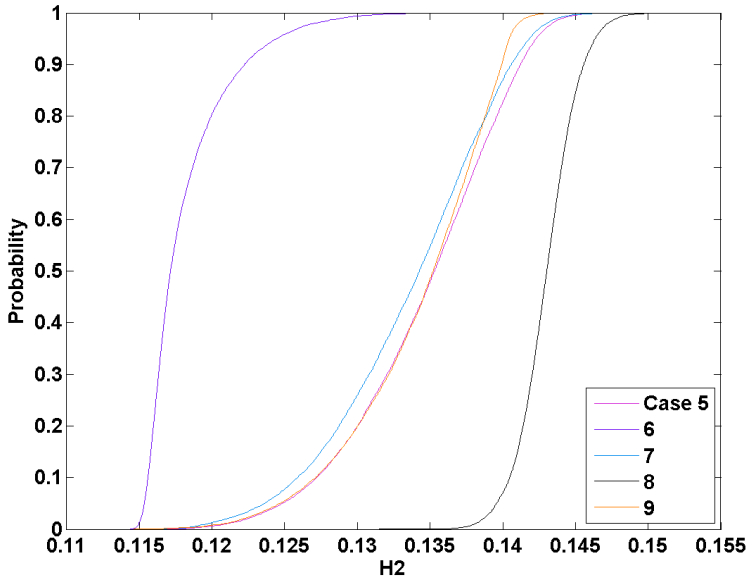

Figure 14 Empirical CDF of posterior distribution of H_2 mole fraction for UQ cases 5-9

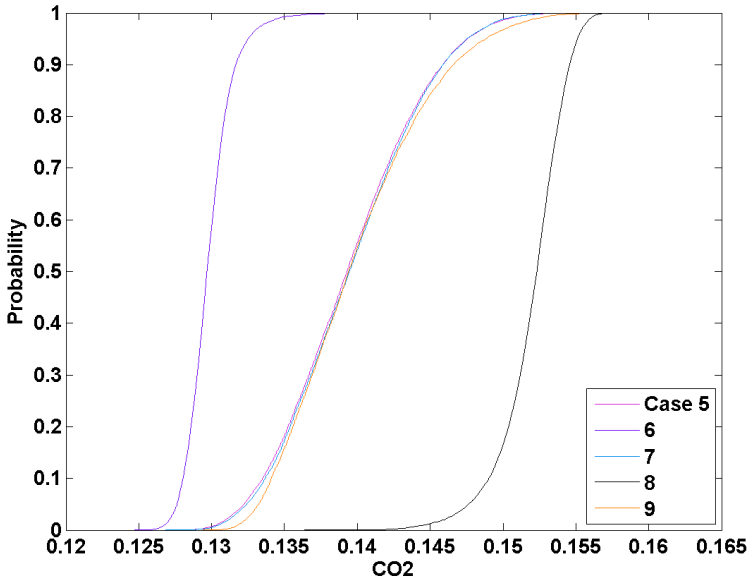

Figure 15 Empirical CDF of posterior distribution of CO_2 mole fraction for UQ cases 5-9

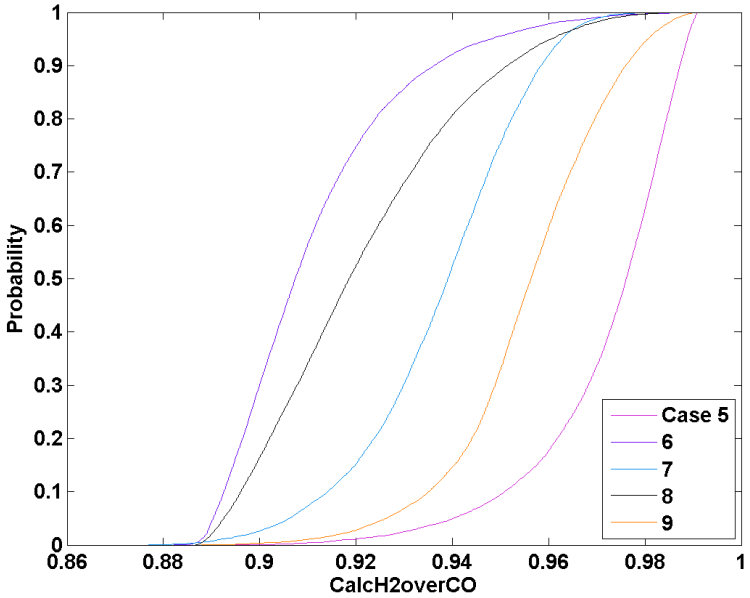

Figure 16 Empirical CDF of posterior distribution of H_2/CO for UQ cases 5-9

It can be observed from Table 5 and Figure 9 through Figure 16 that steam to oxygen ratio has a major impact on syngas composition and the H_2/CO increases with increasing steam to oxygen ratio (cases 6, 5 and 8). For example, if we were to assess the probability of achieving CO mole fraction of 0.1325 or less given the prescribed operating variable uncertainties based on the input uncertainty propagation results shown in Figure 9 through Figure 16, we get different probabilities with small shifts in the mean. Using the eCDF plots for cases 5, 6 and 8, the results can be interpreted in the following way.

For Case 5 (where the mean of steam to oxygen ratio is at the experiment conditions), the probability of observing CO mole fraction less than equal to 0.1325 is about 45%.

For Case 6 where the mean of steam to oxygen ratio was reduced to 0.5 (-30% shift in the mean), the likelihood of achieving same or less CO mole fraction, under the prescribed operating parameter uncertainties, is about 0%.

For Case 8 where the mean of steam to oxygen ratio was is increased to 1.0, the likelihood of achieving same or less CO mole fraction, under the prescribed operating parameter uncertainties, is about 100%.

Additionally, cases 5 and 7 show that increasing the particle size slightly decreases H_2/CO and increasing the coal flow rate (cases 5 and 9) slightly increases H_2/CO. Similar findings were also reported by Karimipour et al. [3].

4.4 IDENTIFICATION OF BEST CANDIDATES FOR NEW EXPERIEMNTS

The preliminary UQ analysis has shown that the choice of sampling method for the experiments have substantial impact in the results and how UQ methods are employed. Given this insight one could probably construct the experimentation plan with different sampling methodology. However, considering the investment already made with the existing experiments by Karimipour et al. [3], we asked the question if we were to update the experimental plan with additional experiments in an incrementally adaptive fashion then what additional sampling locations would be useful?

To answer this question, we framed it as an optimization problem with single objective function, i.e., identify new sampling points for coal flow rate (x_1), coal particle size (x_2) and steam to oxygen ratio (x_3) in the original parameter space such that the uncertainty in CO, H_2 and CO_2 emulators collectively are maximum [7]. The motivation is to add more sample at such locations to reduce the uncertainty. To solve this problem, the objective function for the optimization was set as the collective standard deviation of the three variables. The optimization problem can be represented mathematically as shown in

$$\underset{\boldsymbol{x}}{\boldsymbol{maximize}}$$

$$\boldsymbol{f(x_1, x_2, x_3)} = \sqrt{\boldsymbol{\sigma^2_{CO}}\,(\boldsymbol{x_1, x_2, x_3}) + \boldsymbol{\sigma^2_{H2}}\,(\boldsymbol{x_1, x_2, x_3}) + \boldsymbol{\sigma^2_{CO2}}\,(\boldsymbol{x_1, x_2, x_3})} \qquad \textbf{13}$$

subject to: $0.036 \leq x_1 \leq 0.063$ $\quad 70 \leq x_2 \leq 500$ $\quad 0.5 \leq x_3 \leq 1.0$

A multi-point particle swarm optimizer was used to perform the optimization. The optimization parameters were chosen such that 10 most likely locations with highest objectives could be identified simultaneously in the design space.

The results of the optimization were new sampling locations (x_1, x_2, x_3) identified, which are shown in

Table 6and satisfies the objective and constraints provided above. The GEBHM surrogate model generated in the previous sections were used to evaluate the objective function. As expected by reviewing Figure 3 through Figure 6, the new sampling locations are mostly in the regions were the highest uncertainty in the surrogate is observed (identified with yellow color in the legend bar). For problems like this case with simple factorial based sampling and only few dimensions, one might be able to achieve this qualitatively by reviewing the surface plots as shown in Figure 3 through Figure 6 and adding sampling locations in the regions with highest uncertainty. However, for more complex problems with higher dimensions of uncertain parameters, framing the problem as an optimization problem with single aggregate objective with equal weights (such as to identify the locations that maximize the aggregate standard deviation of all QoIs where each of the QoI can have the same or a distinct weighting factor) or multi-objective will provide a better systematic approach that can improve the results of the experiments.

Factor 1	Factor 2	Factor 3
Coal flow rate (g/s)	Particle size (μm)	H2O/O2 ratio in syngas
0.0360	70	0.831
0.0360	70	0.670
0.0630	76	0.835
0.0630	500	0.810
0.0628	74	0.663
0.0362	493	0.657
0.0360	268	0.580
0.0360	264	0.918
0.0630	302	0.576
0.0360	326	0.584

Table 6 New set of experiments operating parameters identified for sampling based on the assessment of the existing acquired samples

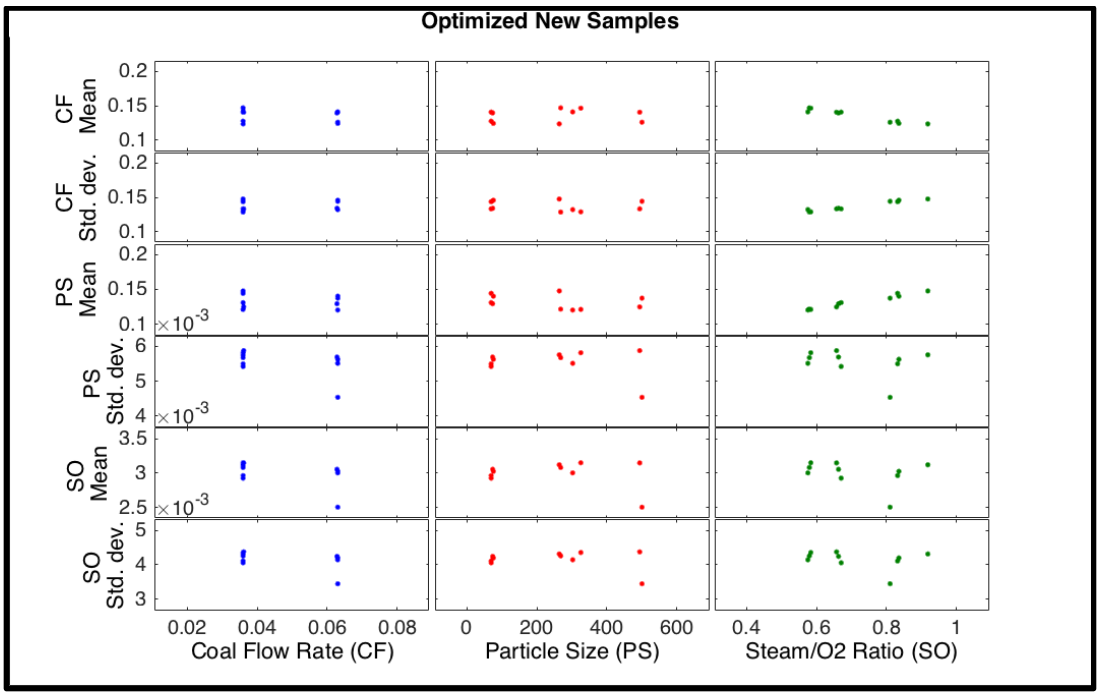

Figure 17 Sampling locations identified which could be used to reduce the uncertainty in the surrogate models if additional experiments were to be conducted

5. COMPUTATIONAL APPROACH

5.1 SAMPLING CFD SIMULATIONS FOR NON-INTRUSIVE UQ ANALYSIS

CFD simulation of reacting multiphase flows are computationally very demanding and require long duration transient simulations to reach statistically significant behavior of the quantities of interest. Hence, for non-intrusive UQ analysis, where a deterministic software is employed for sampling, it is preferred to construct a data-fitted surrogate model that adequately relates the inputs with the quantities of interest. The surrogate model is then used during UQ analysis instead of the actual CFD simulation based evaluations. For this purpose, several dedicated simulation campaigns were performed as part of this research effort at NETL. The simulation campaign employed for the purposes of this study aimed at replicating the physical experiments by running 3D MFIX simulations with the same set of operating conditions (i.e., coal flow rate, coal particle size and steam to oxygen ratio) and range of values. For the physical experiments, Central Composite Design based sampling approach was employed with 20 samples, where 6 of them were replications of the center point operating conditions. The 3D MFIX simulations employed in the current study are deterministic CFD simulations, which implies same results will be obtained when same operating conditions are simulated. Hence, only 15 samples among the 20-sample matrix were used by eliminating the need to perform any replication runs for the replicated samples due to deterministic nature of CFD simulations employed.

The simulation campaigns were carried out on NETL's HPC system, Joule. However, due to the large number of simulations required during the simulation campaigns for the completion of this project, additional high performance computing resources had to be secured through one of the competitive DOE HPC programs. A proposal to the 2014 ASCR Leadership Computing Challenge (ALCC) program of the U.S. Department of Energy's Office of Science led to 38 million CPU hour award at the National Energy Research Scientific Computing Center (NERSC) after peer review. Moreover, a proposal under the 2015 ASCR Leadership Computing Challenge (ALCC) program of the U.S. Department of Energy's Office of Science led to 111.5 million CPU hour award at Argonne Leadership Computing Facility (ALCF) in Argonne National Laboratory of the U.S. Department of Energy.

MPI based distributed-memory implementation of MFIX Two-Fluid Model (MFIX-TFM) was employed to achieve a faster time-to-solution. Due to the transient nature of reacting multiphase flows, each of the sampling simulations were carried out until "quasi-steady state" was reached for the QoIs. Hence, the convergence criteria were based on the assessment for quasi-steady state behavior of the quantities of interest, which were written in a standalone output file at certain frequency. The QoIs employed in GEBHM analysis were obtained by taking the time average for the last user specified duration of simulated time by running a custom Python script, which was developed specifically for this project to handle any number of QoI files under the sampling simulation directories. To ensure time averaging window does not affect the reported QoIs, time averages with several different durations (e.g., for the last 10, 15 & 20 s) were obtained and compared. For example, run #7 took about 50 seconds to reach a quasi-steady state, while run # 9 took about 120 seconds of simulated time to reach quasi-steady state.

Hence, this convergence criteria usually resulted in variability in the total wall clock time required to stop the simulation for each sample under consideration. Such variability in

convergence poses unique challenges when conducting the simulations in a shared HPC resource with batch queuing systems and required several custom workflows to be generated to conduct these simulations efficiently. For example, for many high-performance computing sites such as National Energy Research Scientific Computing (NERSC) Center, which was employed in the current study, bundling all sampling simulations in a single batch job to request more number of cores and longer wall-clock execution time is preferred.

MFiX [5], which is an open source computational fluid dynamics software suite developed and maintained by the U.S. Department of Energy's National Energy Technology Laboratory, was used to model the bench-scale fluidized bed gasifier studied by Karimipour et al. [3]. MFiX is a suite of CFD solvers, which includes both the continuum approach (multi-fluid) and discrete approach (DEM and MPPIC) to multiphase flow modeling (such as gas-solid flows typically encountered in fluidized bed). In this study, the multi-fluid framework in MFiX (i.e., MFiX-TFM solver's 2015-2 release version) has been used. Hence, the gaseous mixture is modeled as a gas-phase and the particulates are modeled as interpenetrating continuous solidphase. Multiple solid-phases can be used to describe multiple particulate materials. In this work, two distinct solid-phases are used to describe coal and sand particles. The governing equations employed for conservation of mass, momentum, energy and species transport for each phase ($m = g$ for gas and $m = s$ for solid) are:

$$\frac{\partial}{\partial t}(\varepsilon_m \rho_m) + \nabla . (\varepsilon_m \rho_m \vec{V}_m) = \sum_{n=1}^{N} R_{mn} \quad \textbf{14}$$

$$\frac{\partial}{\partial t}(\varepsilon_m \rho_m \vec{V}_m) + \nabla . (\varepsilon_m \rho_m \vec{V}_m \vec{V}_m) = \nabla . \overline{\overline{\tau_m}} - \epsilon_m \nabla P + \varepsilon_m \rho_m \vec{g} + \sum_n \overrightarrow{I_{mn}} \quad \textbf{15}$$

$$\varepsilon_m \rho_m C_{pm} \left(\frac{\partial T_m}{\partial t} + \vec{V}_m . \nabla T_m\right) = -\nabla . \overrightarrow{q_m} + \sum_n \gamma_{mn}(T_n - T_m) - \Delta H_{rm} \quad \textbf{16}$$

$$\frac{\partial}{\partial t}(\varepsilon_m \rho_m X_{ml}) + \nabla . (\varepsilon_m \rho_m X_{ml} \vec{V}_m) = R_{ml} \quad \textbf{17}$$

Where subscripts m and n represent phases and l represents a species in a phase. The closure terms for the solid phases are obtained through kinetic granular theory with an algebraic form of the granular temperature equation. The Schaeffer frictional model was used in the dense regions and the Gunn's correlation was used for heat transfer.

The momentum transfer between the gas and solid phases are modeled using Gidaspow drag model in MFIX-TFM. Detailed information on the constitutive relations used to model momentum and energy exchange terms between the phases along with solid stress model used in MFiX can be obtained in MFiX online documentation [17], [18].

5.2 REACTION MODEL

Coal devolatilization and gasification reaction kinetics are obtained from Niksa Energy Associates LLC computer software PC Coal Lab [19]. PC Coal Lab provides the complete char conversion history of coal, along with appropriate molar stoichiometric coefficients and kinetic constants for devolatilization and gasification reaction rates at a user-specified reactor pressure, temperature & gas composition. Pyrolysis process decomposes volatile matter into various species with the devolatilization reaction shown in Eq. (18) with the rate given by Eq. (25) in Table 8.

$$\boldsymbol{VM \rightarrow n_{CO_2} CO_2 + n_{CO}\, CO + n_{H_2}\, H_2 + n_{CH_4}\, CH_4 + n_{H_2O}\, H_2O + n_{H_2S}\, H_2S + n_{C_3H_6}\, C_3H_6 + n_{HCN}\, HCN + n_{C_2H_6}\, C_2H_6 + n_{C_2H_4}\, C_2H_4 + n_{TAR}\, TAR} \quad \textbf{(18)}$$

The molar stoichiometric coefficients for devolatilization use in this work are

$n_{CO_2} = 0.132,\ n_{CO} = 0.116,\ n_{H_2} = 0.019,\ n_{CH_4} = 0.107,\ n_{H_2O} = 0.302, n_{H_2S} = 0.013,$
$n_{C_3H_6} = 0.012,\ n_{HCN} = 0.005,\ n_{C_2H_6} = 0.004,\ n_{C_2H_4} = 0.023, n_{TAR} = 0.064.$

Gasification Reactions

Steam and carbon dioxide are used as gasification agents to produce carbon monoxide and hydrogen according to Eqs. (19) and (20). The gasification reaction rate expressions, Eqs. (28) and (29) in Table 8, are obtained from PC Coal Lab [19].

$$\boldsymbol{C + H_2O \rightarrow CO + H_2} \quad \textbf{(19)}$$

$$\boldsymbol{C + CO_2 \rightarrow 2CO} \quad \textbf{(20)}$$

Local gas composition inside a gasifier can vary significantly and presence of CO and H_2 inhibits gasification reactions, the kinetic constants for the gasification reactions are obtained for a range of gas composition (CO, CO_2, H_2, H_2O) at the reactor operating pressure and temperature. To achieve this, a design of experiment was carried out in order to construct 500 samples of PC Coal Lab simulations, covering the parametric space for mole fraction of CO, CO_2, H_2, H_2O changing between 0 and 0.25, which is the upper range of expected mole fraction for our syngas composition. An analysis of the 500 set of kinetic constants generated (pre-exponent, activation energy, order of reaction and annealing factor) exhibits a strong correlation between the kinetic constants and hydrogen mole fraction. The kinetic constants in Eqs. (28) and (29) are given by Table 7.

Oxidation Reactions

Char oxidation reaction, Eq. (21), which is an exothermic reaction, is modeled using the shrinking core gas-solid particle reaction model proposed by Field et al. [20] with the reaction rate given by Eq. (27) in Table 8.

$$\boldsymbol{C + \frac{1}{2} O_2 \rightarrow CO} \quad \textbf{(21)}$$

In Field et al. [20], A_{char} and E_{char} are given as 8,710 gm/atm-cm^2-s and 35,700 cal/gmole, respectively. To investigate the effect of char oxidation reaction model on syngas composition, the kinetic reaction model of DeSai and Wen [21], where A_{char} and E_{char} oxidation are given as 8,710 gm/atm-cm^2-s and 27,000 cal/gmole respectively was also tested. Gas phase reactions are described using simple global reaction mechanisms.

Carbon monoxide oxidation model, Eq. (22), is treated as a categorical uncertain model, so the effect of carbon monoxide oxidation on syngas composition can be investigated. The reaction models proposed by Howard [22], Eq. (30), and Westbrook and Dryer [23], Eq. (31), are used in the present work.

$$\boldsymbol{CO + \frac{1}{2} O_2 \rightarrow CO_2} \quad \textbf{(22)}$$

Hydrogen oxidation reaction model, Eq. (23), proposed by Peters [24] and methane oxidation reaction model, Eq. (24), proposed by Dryer and Glassman [25] are used to model hydrogen and methane oxidation with the reaction rates provided by Eqs. (32) and (33) in Table 8, respectively.

$$\boldsymbol{2H_2 + O_2 \rightarrow 2H_2O} \quad \textbf{(23)}$$

$$\boldsymbol{CH_4 + 2O_2 \rightarrow CO_2 + 2H_2O} \quad \textbf{(24)}$$

Water Gas Shift Reaction

Since water gas shift reaction model, Eq. (25)(25)(25)(25) is also treated as a categorical uncertain input parameter, the reaction models of Chen et al. [26] and Biba et al. [27] are used to account for conversion of carbon monoxide and steam to hydrogen and carbon dioxide, where the reaction rates are given by Eqs. (34) and (35), respectively.

$$\boldsymbol{CO + H_2O \leftrightarrow CO_2 + H_2} \quad \textbf{(25)}$$

Coal particles undergoing mass transfer due to moisture release, devolatilization and chemical reactions become more porous, as char conversion progresses. The solid phase accounts for interface mass transfer by reducing the particle material density.

Steam gasification

X_{h_2}	$\gamma_{h_2o} A_{h_2o}$ $(\frac{mole}{cm^3 s})$	E_{h_2o} $(\frac{cal}{mole})$	n_{h_2o}	k_{h_2}
$4.0e^{-2} \geq X_{H_2}$	1.249	23300	0.93	0
$4.0e^{-2} < X_{h_2} < 2$	$1.619\ e^{2.64\ X_{h_2}}$	$24249 + 7995\ X_{h_2} - 1382\ X_{h_2}^2 + 161 X_{h_2}^3 - 9\ X_{h_2}^4$	0.98	22.5
$2 \leq X_{h_2} \leq 5$	$14.026\ X_{h_2}^{4.04}$	$24249 + 7995\ X_{h_2} - 1382\ X_{X_{h_2}}^2 + 161\ X_{X_{h_2}}^3 - 9\ X_{X_{h_2}}^4$	0.98	22.5
$5 < X_{h_2}$	$47.08\ X_{h_2}^{3.45}$	$32683 + 7480 \log(X_{h_2})$	1	$22.786 + 0.037 * X_{h_2}$

Carbon dioxide gasification

X_{h_2}	$\gamma_{co_2} A_{co_2}$ $(\frac{mole}{cm^3 s})$	E_{co_2} $(\frac{cal}{mole})$	n_{co_2}	k_{co}
$4.0e^{-2} \geq X_{h_2}$	33.38	40400	0.98	0
$4.0e^{-2} < X_{h_2} < 2$	$52.963\ e^{2.37\ X_{h_2}}$	$41426 + 8102\ X_{h_2} - 1454\ X_{h_2}^2 + 169 X_{h_2}^3 - 9\ X_{h_2}^4$	1.0	$0.7598 - 0.1804\ X_{h_2} + 0.0362\ X_{h_2}^2 - 0.005 X_{h_2}^3 + 0.0003\ X_{h_2}^4$
$2 \leq X_{h_2} \leq 5$	$4000\ X_{h_2}^{3.47}$	$41426 + 8102\ X_{h_2} - 1454\ X_{h_2}^2 + 169 X_{h_2}^3 - 9\ X_{h_2}^4$	1.0	$0.7598 - 0.1804\ X_{h_2} + 0.0362\ X_{h_2}^2 - 0.005 X_{h_2}^3 + 0.0003\ X_{h_2}^4$
$5 < X_{h_2}$	$20000\ X_{h_2}^{2.7}$	$49661 + 7485 \log(X_{h_2})$	1	$0.6113 - 0.0779\ X_{h_2} + 0.0057\ X_{h_2}^2 - 0.0002 X_{h_2}^3 + 3e^{-6}\ X_{h_2}^4$

Table 7 Kinetic values used in the rate expression for steam and CO_2 gasification

$$r_{pyrolysis} = \varepsilon_p \, 36,000 \exp\left(\frac{-9,060}{R\,T_p}\right) \frac{\rho_p Y_{vm}}{MW_{vm}} \quad (26)$$

$$r_{co} = \frac{-3\varepsilon_s P_{o_2}}{d_p\left(\frac{1}{k_{film}}+\frac{1}{k_{ash}}+\frac{1}{k_{reaction}}\right)MW_{o_2}} \quad (27)$$

$$k_{film} = \frac{D_{o_2} Sh}{d_p \frac{R}{MW_{o_2}} T_g}$$

$$k_{ash} = \frac{2 r_d D_{eff_{ash}}}{d_p\,(1-r_d)\frac{R}{MW_{o_2}} T_s}$$

$$k_{reaction} = A_{char} \exp\left(-\frac{E_{char}}{RT_s}\right) r_d^2$$

$$r_{h_2o} = \gamma_{h_2o} A_{h_2o} \exp\left(\frac{-E_{h_2o}}{RT}\right) \frac{\varepsilon_s \rho_s Y_{Char}}{MW_{Char}} \frac{p_{h_2o}^{n_{h_2o}}}{(1-K_{h_2} p_{H_2})} \quad (28)$$

$$r_{co_2} = \gamma_{co_2} A_{co_2} \exp\left(\frac{-E_{co_2}}{RT}\right) \frac{\varepsilon_s \rho_s Y_{Char}}{MW_{Char}} \frac{p_{co_2}^{n_{co_2}}}{(1-K_{co} p_{co})} \quad (29)$$

$$r_{co} = 1.3x10^{14} \exp\left(-\frac{30,000}{RT_g}\right) \varepsilon_g \, C_{o_2}{}^{0.5} C_{co} \, C_{h_2o}{}^{0.5} \quad (30)$$

$$r_{co} = 3.98x10^{14} \exp\left(-\frac{20,130}{RT_g}\right) \varepsilon_g \, C_{o_2}{}^{0.25} C_{co} \, C_{h_2o}{}^{0.5} \quad (31)$$

$$r_{h_2} = 1.08x10^{16} \exp\left(-\frac{30,000}{RT_g}\right) \varepsilon_g C_{o_2} \, C_{h_2} \quad (32)$$

$$r_{ch_4} = 1.58x10^{13} \exp\left(-\frac{48,400}{RT_g}\right) \varepsilon_g \, C_{o_2}{}^{0.8} C_{ch_4}{}^{0.7} \quad (33)$$

$$r_{wgs} = A_{wgs} \exp\left(-\frac{21,700}{RT_g}\right) \left(P_{co} P_{h_2o} - \frac{P_{h_2} P_{co_2}}{0.0265\, e^{\frac{3956}{Tg}}}\right) \quad (34)$$

$$r_{wgs} = 2,780 \exp\left(-\frac{3,010}{RT_g}\right) \left(C_{co} C_{h_2o} - \frac{C_{h_2} C_{co_2}}{0.029\, e^{\frac{4094}{Tg}}}\right) \quad (35)$$

Table 8 Reaction models for the heterogeneous and homogeneous reactions

5.3 SIMULATION CAMPAIGN BASED ON CENTRAL COMPOSITE DESIGN

The target of first set of simulations was the exact replication of the physical experiments by using the same statistical design of experiments generated operating conditions as shown in the Table 9. Although such experiment matrix is more suited for physical experiments rather than computer experiments, the same matrix was replicated for CFD simulations. Hence, 15 distinct MFIX-TFM simulations were set up by changing the three operating variables used in the physical experiments in Karimipour et al. [3]. As MFIX simulations are deterministic in nature, the six-replicated experiment runs for the center point in the CCD sampling method was represented as single simulation using the same operating conditions. The QoIs were calculated by temporal averaging for the last 10 seconds of the simulation for each sample.

5.3.1 Simulation results

The time averaged mole fraction values for CO and H_2 from MFIX-TFM simulation (Solid Square) and measurement from experiments (asterisk) are shown in Figure 18. Both values of time averaged CO and H_2 mole fraction are under-predicted at some of the sampling runs and over-predicted at other sampling runs. In order to better quantify the uncertainty in the predicted syngas mole fraction, GEBHM analysis was used to predict the uncertainty band associated with the time averaged values of syngas composition.

Figure 19 to Figure 21 show the parity plots for the emulator's prediction (y-axis) vs. experimental results (x-axis) for CO, H_2 and CO_2 mole fractions respectively. Values on the diagonal line indicate perfect agreement between the predictions from the constructed surrogate and experiment. The blue solid circles in these figures represent the emulator's prediction of mole fraction values for the syngas species under consideration at the experiment sampling locations. The intervals represent the uncertainty bands due to propagation of uncertainties in the three input uncertain parameters (coal flow rate, particle diameter and steam to oxygen ratio). The difference between the solid circle symbols and the diagonal line (actual species mole fraction) is the discrepancy. The red solid squares in Figure 19 to Figure 21 are the emulator's prediction, after they are corrected for the model discrepancy as part of the GEBHM analysis. It can be seen that the magnitude of the discrepancy varies depending on the values of the uncertain input parameters. The discrepancy function distribution as a function of steam to oxygen ratio for CO, H_2 and CO_2 mole fractions are shown in Figure 22 through Figure 24. A positive value on the y-axis indicates the amount of under-prediction in the syngas composition, whereas a negative value on y-axis indicates the amount of over-prediction in the syngas composition. Hydrogen mole fraction is under-predicted across the entire operating conditions. The trend observed in predicted values of CO mole fraction is changing from under-predication (at lower steam to oxygen ratio) to over-predication at higher steam to oxygen ratio. The opposite trend is observed in the predicted CO_2 mole fraction behavior. Response surface plots based on the emulators were constructed with the sampling simulation results obtained with MFIX runs. Figure 25 through Figure 27 shows the response surface plots for CO, H_2 and CO_2 mole fractions as function of steam to oxygen ratio and coal particle size, where coal flow rate was kept at a nominal setting for illustration purposes. The emulators were constructed based Gaussian

Process Model (GPM) in order to establish a model that approximates the relationship between the three input factors and quantities of interest using the sampling simulation data.

	Uncertain Input Parameters/Factors			Primary Quantities of Interest (Response Variables)				
Actual order of experiment	Factor 1	Factor 2	Factor 3	Response 1	Response 2	Response 3	Response 4	Response 5
	Coal flow rate (gr/s)	Particle size (μm)	H_2O/O_2 ratio in syngas	Carbon conversion	H_2/CO ratio in syngas	CH_4/H_2 ratio in syngas	Gasification efficiency	Gas yield (m^3/kg-coal)
1	0.063	70	0.5	91.57%	0.81	0.065	56.50%	3.45
2	0.063	70	1	93.35%	1.25	0.052	57.92%	3.57
3	0.0495	70	0.75	92.56%	1.05	0.057	59.03%	3.47
4	0.036	70	0.5	92.26%	0.82	0.066	59.83%	3.42
5	0.036	70	1	93.61%	1.23	0.052	61.17%	3.54
6	0.063	285	0.75	96.59%	1.04	0.058	62.24%	3.63
7	0.0495	285	0.5	93.79%	0.81	0.065	63.93%	3.5
8	0.0495	285	0.75	95.48%	1.01	0.059	62.12%	3.57
9	0.0495	285	0.75	96.00%	1.01	0.057	62.24%	3.61
10	0.0495	285	0.75	96.00%	0.99	0.058	60.79%	3.6
11	0.0495	285	0.75	96.00%	0.98	0.057	66.88%	3.65
12	0.0495	285	0.75	96.89%	1.00	0.059	64.07%	3.66
13	0.0495	285	0.75	96.42%	1.01	0.059	63.66%	3.65
14	0.0495	285	1	95.41%	1.22	0.053	59.50%	3.63
15	0.036	285	0.75	95.68%	1.01	0.057	61.37%	3.59
16	0.063	500	0.5	91.10%	0.81	0.067	56.23%	3.44
17	0.063	500	1	94.33%	1.27	0.054	58.98%	3.6
18	0.0495	500	0.75	93.83%	1.02	0.061	58.84%	3.56
19	0.036	500	0.5	93.58%	0.78	0.070	59.42%	3.47
20	0.036	500	1	96.41%	1.19	0.055	62.94%	3.63
			Mean	94.54%	1.01	0.059	60.88%	3.56
			Standard deviation	1.78%	0.16	0.005	2.70%	0.08
Additional validation experiments								
V1	0.063	500	0.75	92.81%	1.07	0.057	57.66%	3.52
V2	0.036	500	0.75	96.49%	1.01	0.059	62.73%	3.59
V3	0.063	70	0.75	94.45%	1.01	0.058	59.96%	3.55
V4	0.036	70	0.75	95.85%	1.00	0.060	62.00%	3.58

Table 9 Tabulated data for input and primary quantities of interest (response) from experiments [3]

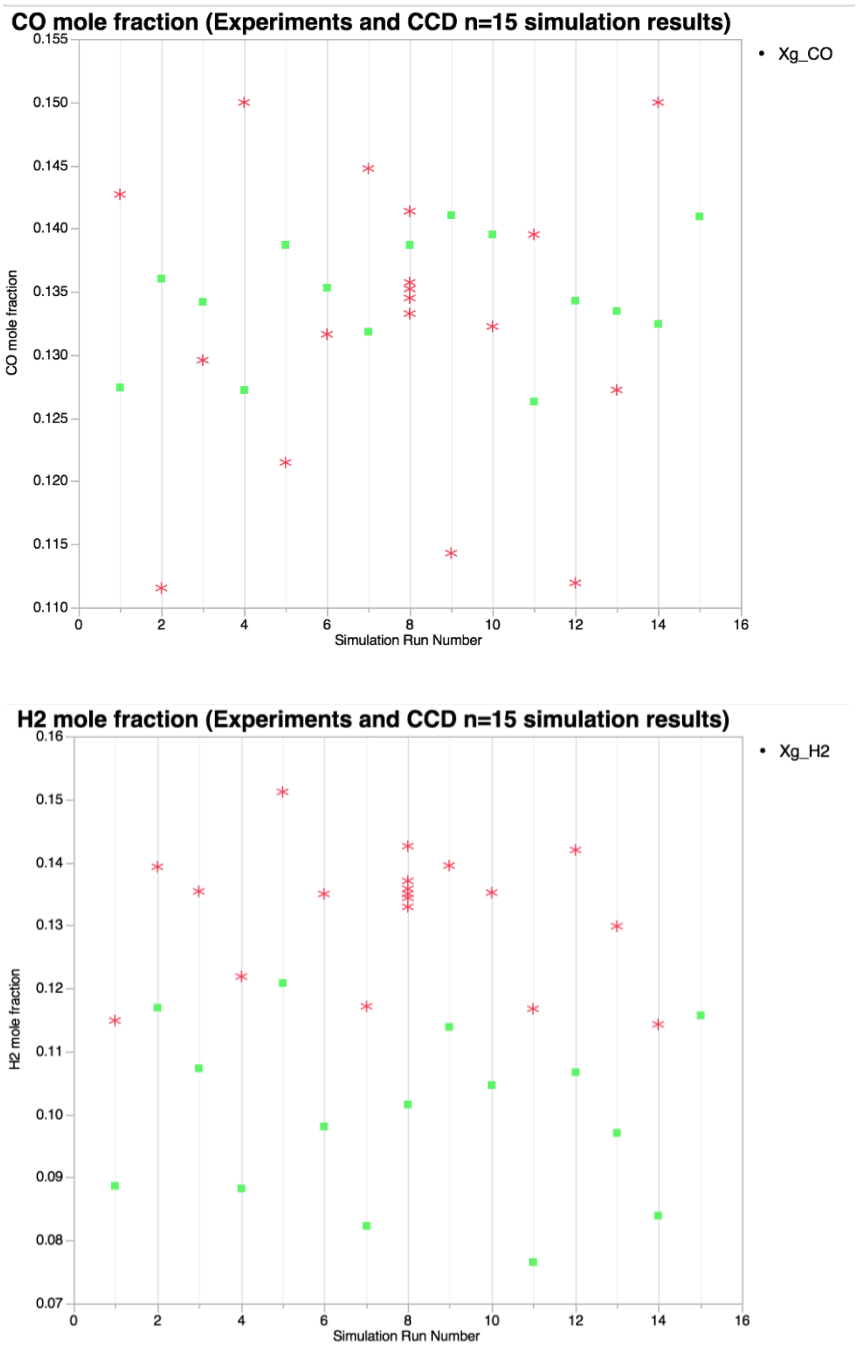

Figure 18 Comparison of 3D MFIX simulation results for each sampling simulation with respect to corresponding experimental data (Green circles are for 3D MFIX simulations. Red asterisk denotes the experiments)

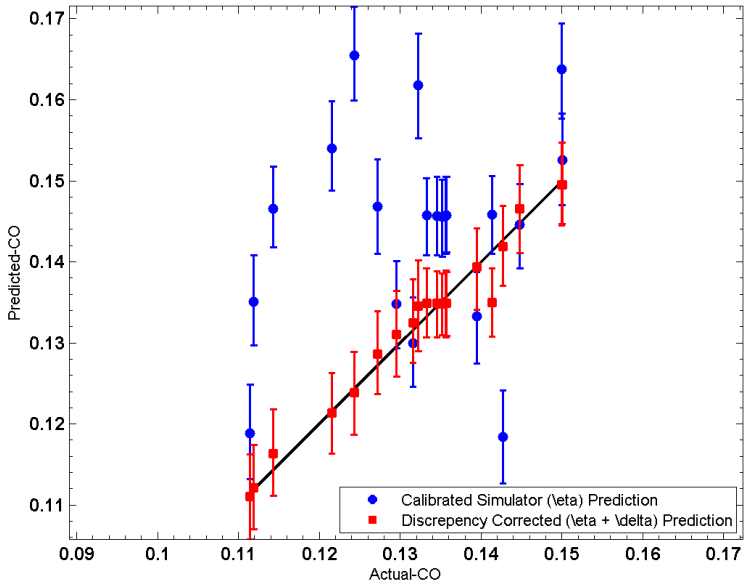

Figure 19 GEBHM surrogate model (emulator) quality for CO mole fraction

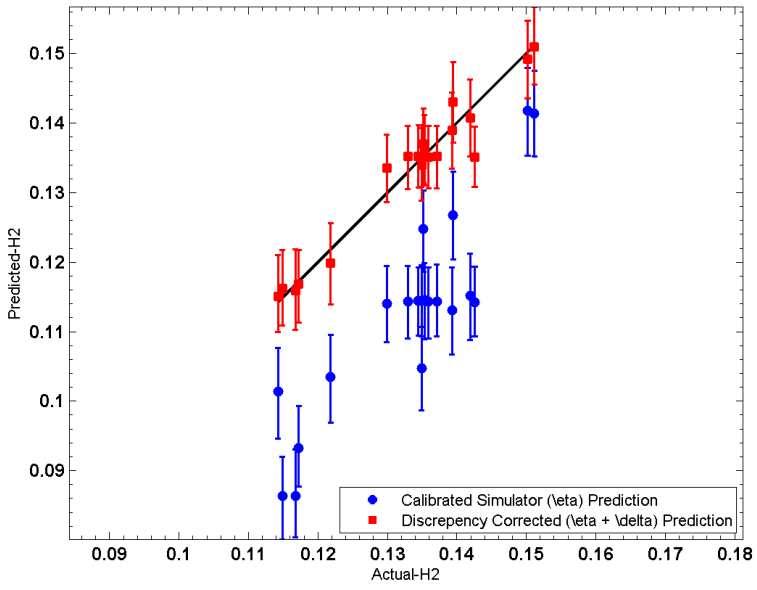

Figure 20 GEBHM surrogate model (emulator) quality for H_2 mole fraction

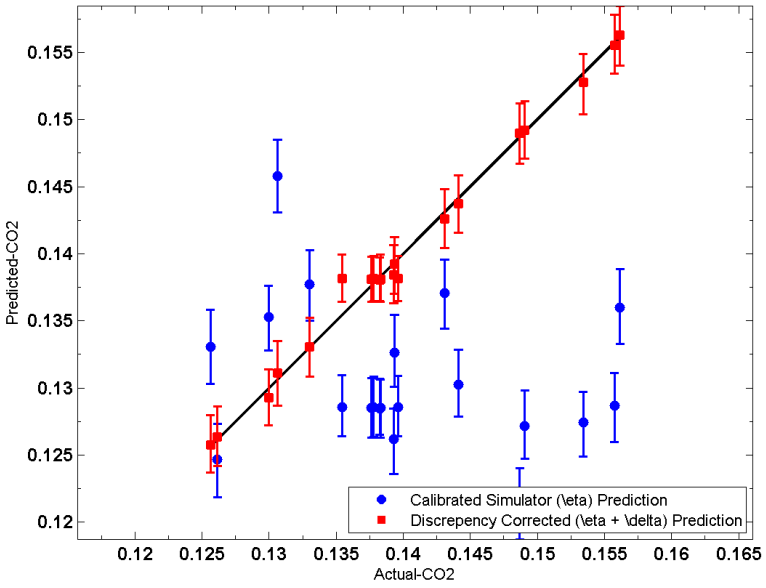

Figure 21 GEBHM surrogate model (emulator) quality for CO_2 mole fraction

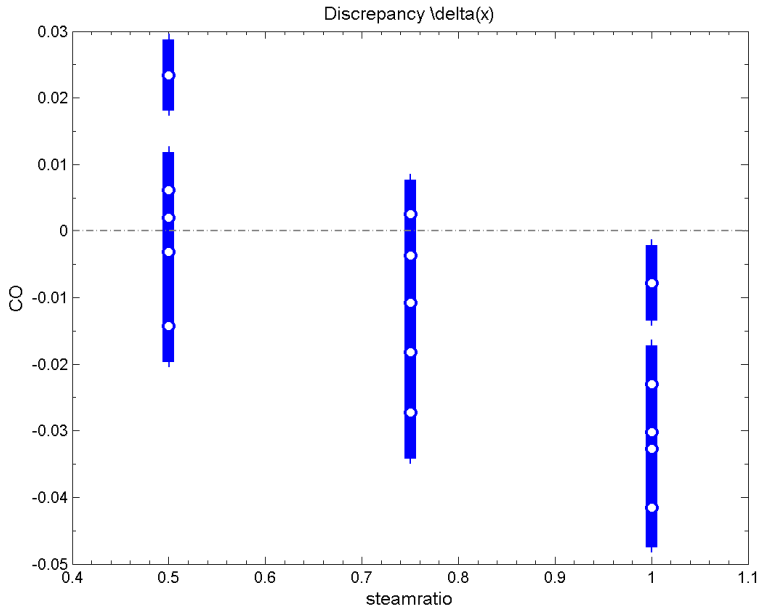

Figure 22 GEBHM discrepancy function distribution for CO surrogate model

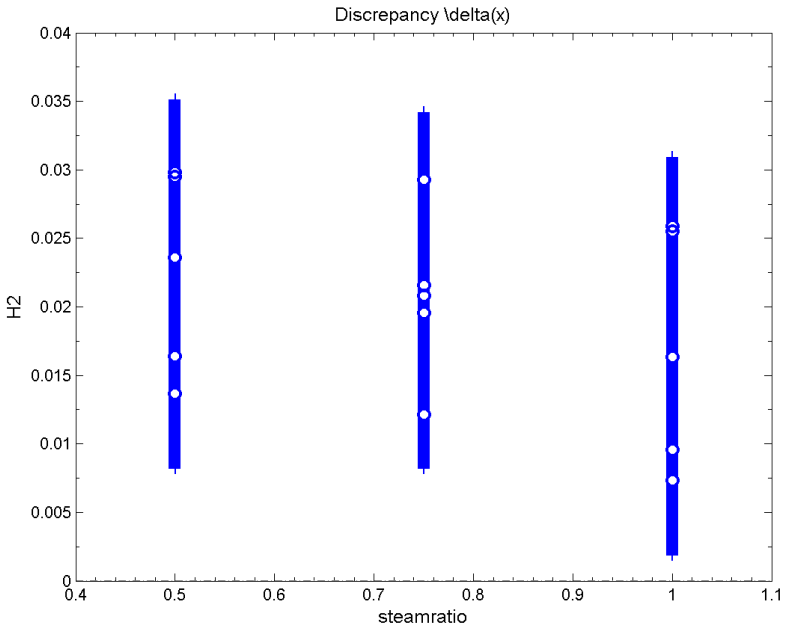

Figure 23 GEBHM discrepancy function distribution for H_2 surrogate model

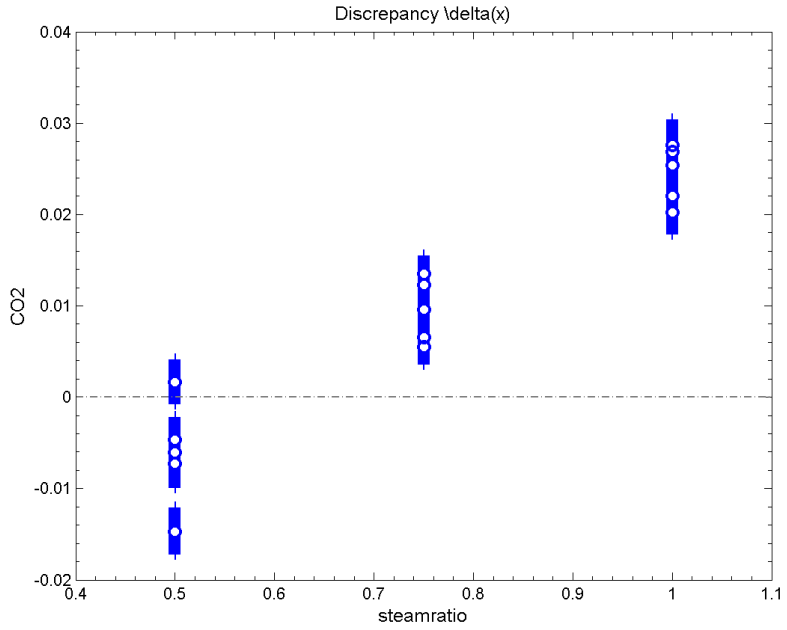

Figure 24 GEBHM discrepancy function distribution for CO_2 surrogate model

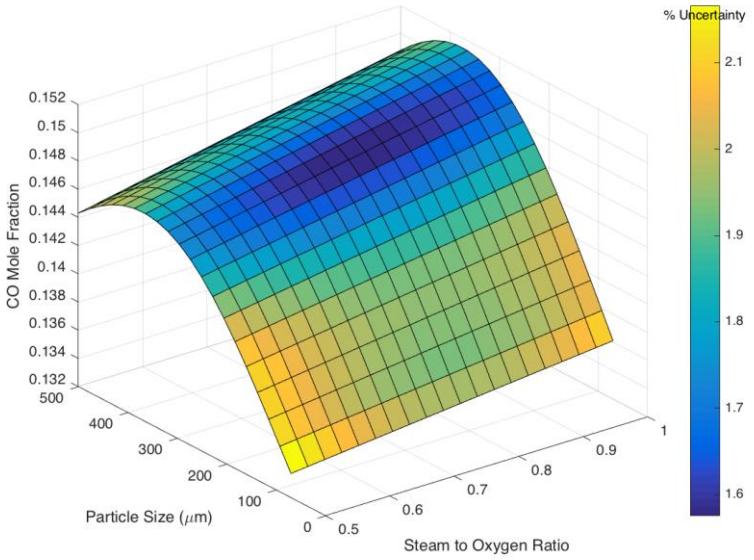

Figure 25 Response surface plot of the surrogate model (emulator) behavior for CO mole fraction (coal flow rate set at midpoint of 0.0495 g/s).

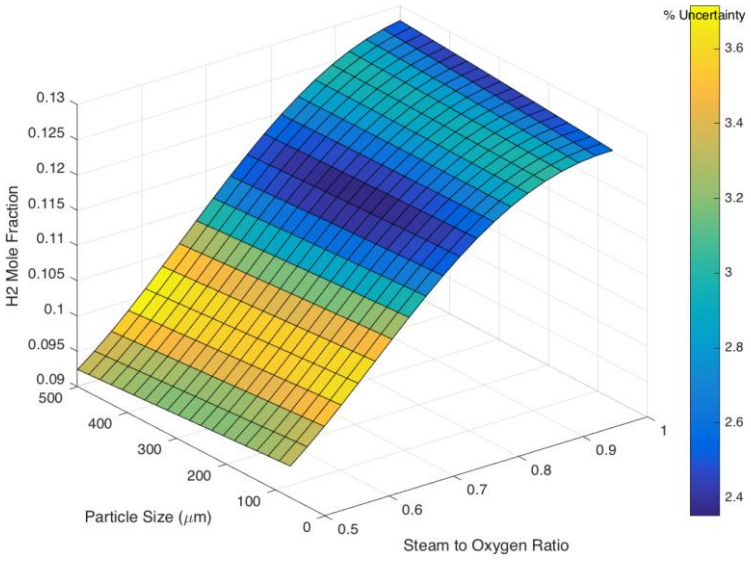

Figure 26 Response surface plot of the surrogate model (emulator) behavior for H_2 mole fraction (coal flow rate set at midpoint of 0.0495 g/s).

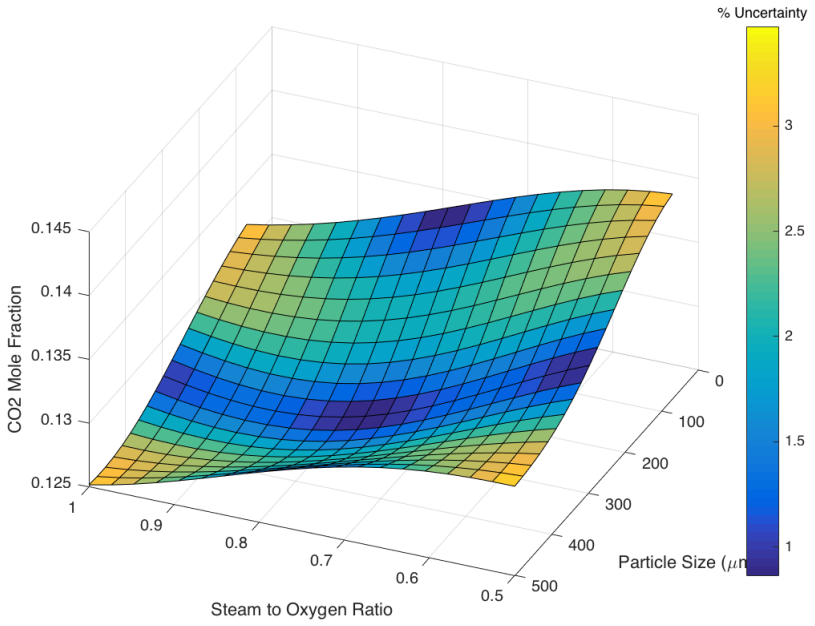

Figure 27 Response surface plot of the surrogate model (emulator) behavior for CO_2 mole fraction (coal flow rate set at midpoint of 0.0495 g/s).

5.3.2 Sensitivity analysis

GEBHM analysis shown earlier for the experimental data in Section 4.2 was replicated for the 3D MFIX simulation results. The global sensitivity analysis results shown in Table 10 is for the same QoIs used in the experiment but this time using MFIX simulation results instead of experimental data standalone. It can be seen that the variability in the predicted syngas composition is largely due to coal flow rate for CO mole fraction, whereas for H_2 it is primarily due to steam to oxygen ratio. The variability in CO_2 mole fraction, however, is due to all three input parameters. Observed trends in Table 10 is contrary to the trends observed with the experimental data in Table 3 where the steam to oxygen ratio was the primary driver for variability observed in QoIs.

To further investigate this discrepancy, sensitivity of CO, H_2, and CO_2 to variance in each of the primary input parameters (coal flow rate, particle diameter and steam to oxygen ratio) was analyzed utilizing one of the features in the GEBHM analysis as shown in Figure 28 through Figure 30. Unlike what was observed in the experimental data, Figure 8, changes in each of the input parameters affect the mole fraction of CO, H_2 and CO_2. For example, there is a large variance in sensitivity of CO to particle flow rate that is caused by variability in particle diameter and steam to oxygen ratio or the variance in sensitivity of CO to particle diameter is affected by variability in coal flow rate and steam to oxygen ratio. The differences observed in the sensitivity analysis of the experimental and predicted syngas composition indicates that the fluidization behavior maybe different in simulations than in the experiment, since coal flow rate and particle diameter can directly affect the hydrodynamics through drag force between gas and

solid phases. The effect that coal flow rate exhibits on syngas composition can further be observed in Figure 31 and Figure 32. Figure 31 shows the time averaged reaction rates for the oxidation reactions, char combustion and char gasification reactions for run numbers 6 and 10 (refer to Table 9). It is clear that adding more coal to the gasifier (going from run number 10 to run number 6) leads to an increase in all the reaction rates. It is also evident that CO oxidation is stronger than char oxidation for both run numbers 6 and 10. Mole fraction of CO, H_2 and CO_2 (measured and predicted) for run numbers 6 and 10 are shown in Figure 32, which points to a decrease in predicted mole fraction of CO, H_2 and an increase in predicted mole fraction of CO_2 when coal flow rate into the gasifier increases. Based on the trends observed in Figure 31 and Figure 32, one can conclude that the extend of the homogeneous CO and H_2 oxidation reactions in the bed is greater than the extend of heterogeneous reactions taking place when coal flow rate is increased. Additionally, Table 10 and Figure 28 through Figure 30 show that CO mole fraction is not sensitive to steam to oxygen ratio. This indicates that, in simulation, coal combustion reaction is not greatly affected by increasing or decreasing the oxygen flow into the gasifier. Therefore, the fluidization and mixing behavior in the experiment have to be somewhat different than the hydrodynamic behavior that the model is predicting.

	Factor 1	Factor 2	Factor 3
	CF	PS	H_2O/O_2
CF: coal flow rate (g/s)	84.7%	0.57%	0.0%
PS: particle size (μm)		14.1%	0.0%
H_2O/O_2 ratio in syngas			0.6%

% Contribution of variability seen in CO mole fraction

	Factor 1	Factor 2	Factor 3
	CF	PS	H_2O/O_2
CF: coal flow rate (g/s)	26.7%	0.02%	1.2%
PS: particle size (μm)		0.1%	0.1%
H_2O/O_2 ratio in syngas			71.9%

% Contribution of variability seen in H_2 mole fraction

	Factor 1	Factor 2	Factor 3
	CF	PS	H_2O/O_2
CF: coal flow rate (g/s)	36.5%	2.11%	3.1%
PS: particle size (μm)		27.9%	2.1%
H_2O/O_2 ratio in syngas			27.6%

% Contribution of variability seen in CO_2 mole fraction

Table 10 Global Sensitivity of Quantities of Interest with respect operating variables based on 3D MFIX simulations with CCD sampling

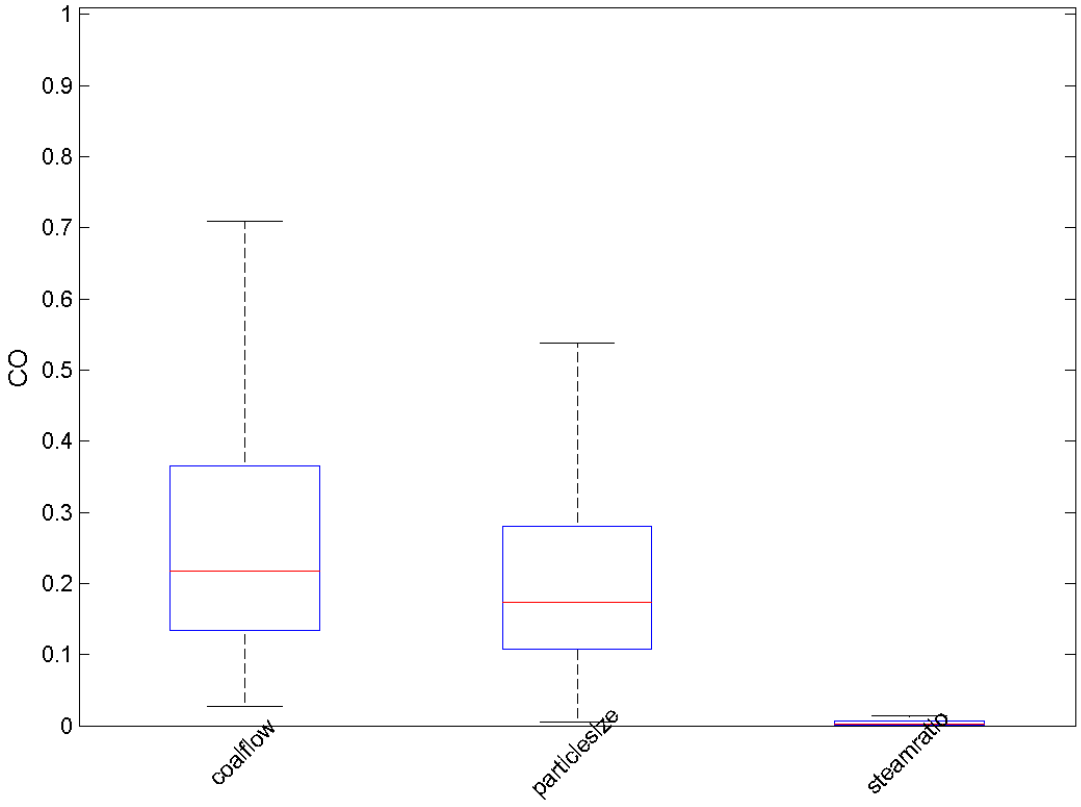

Figure 28 Variance of global sensitivity for CO mole fraction based on MFIX simulation results

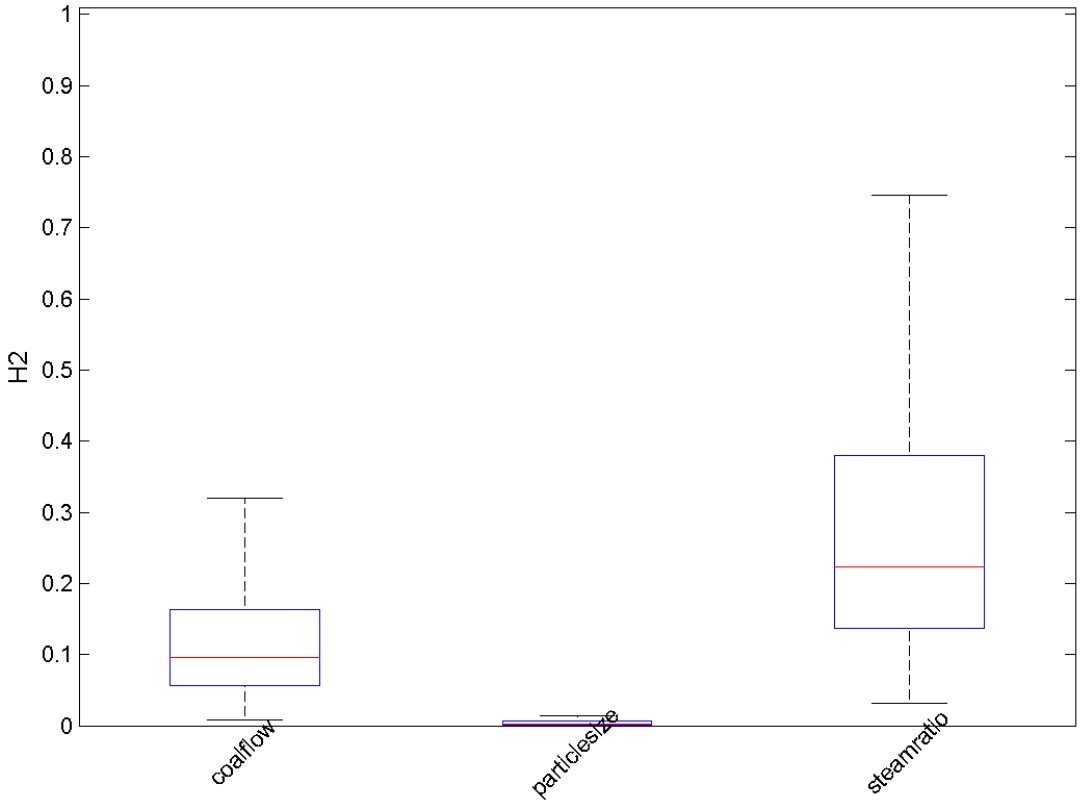

Figure 29 Variance of global sensitivity for H_2 mole fraction based on MFIX simulation results

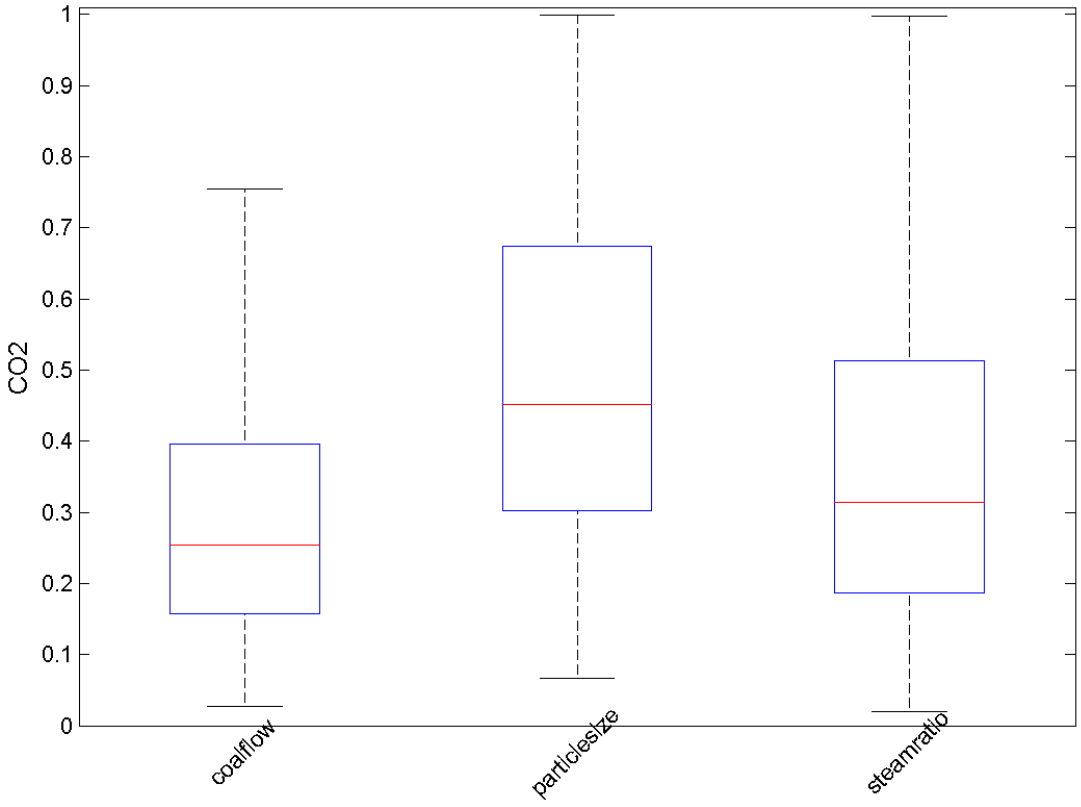

Figure 30 Variance of global sensitivity for CO_2 mole fraction based on MFIX simulation results

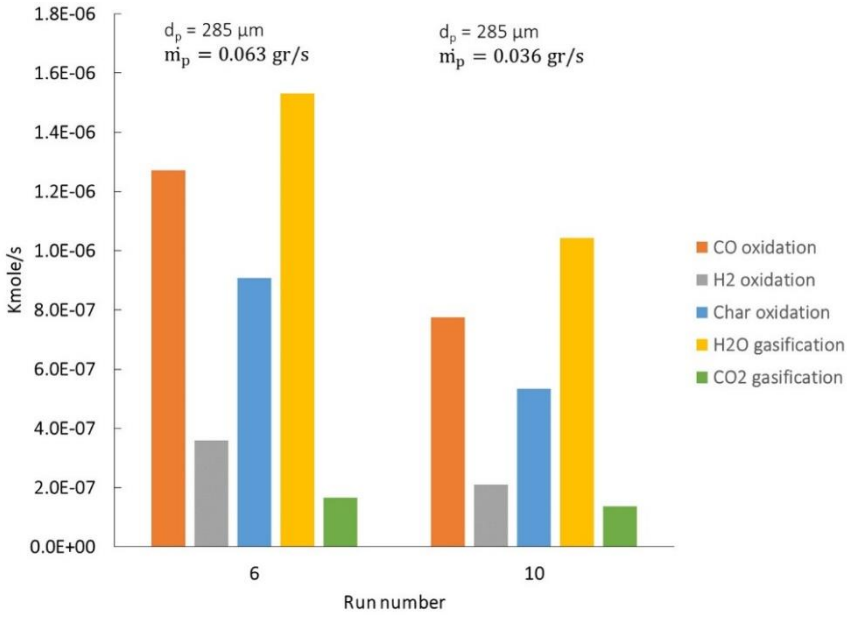

Figure 31 Time averaged predicted reaction rates for run numbers 6 and 10.

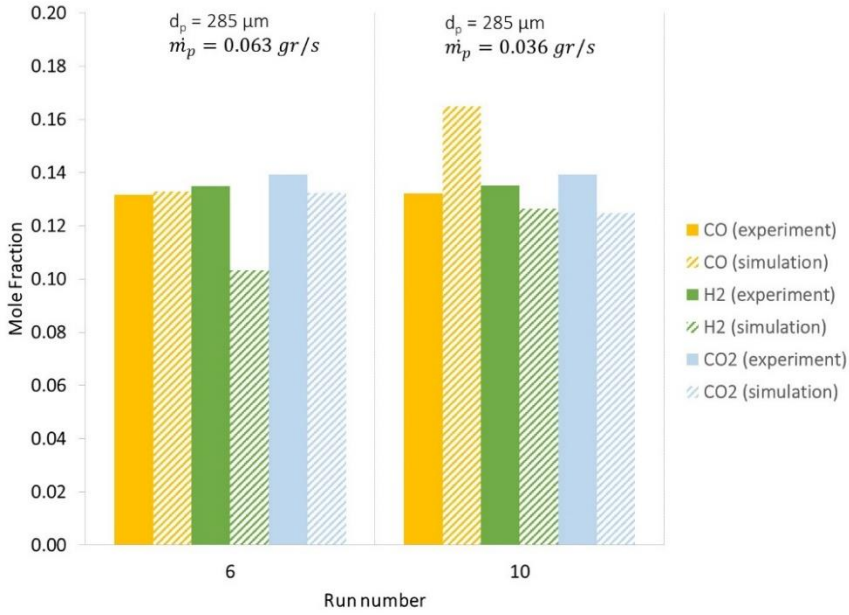

Figure 32 A comparison between the CO and H_2 composition for run numbers 6 and 10, both predicted and measured

5.4 GRID RESOLUTION

As seen in previous section when compared to experimental data, CO mole fraction was under-predicted at lower steam to oxygen ratio and over-predicted at higher steam to oxygen ratio. The opposite trend was observed for CO_2 mole fraction. To improve quality of numerical models used in simulations of a fluidized bed gasifier at any scale, the sources of uncertainty in the simulation have to be identified and quantified. There are several sources of uncertainty that can affect any simulation result and scale up process such as uncertainty in the model input values, uncertainty in the reaction models and kinetic rates, uncertainty in selection of the appropriate numerical models affecting the hydrodynamics, uncertainty in selection of adequate computational grid resolution, uncertainty in the selection of proper numerical techniques required for solution of the discretized conservation equations and many more. The lack of agreement in the CO and CO_2 trend with respect to steam to oxygen ratio that was discussed in the previous section highlights the need to examine uncertainty in reaction models and the effect of computational grid resolution that may affect the hydrodynamics and syngas generation in the fluidized bed. A separate study was carried out, which is presented in this section to show the effect that reaction models for gasification, char oxidation, carbon monoxide oxidation and water gas shift will have on the syngas composition at different grid resolution, along with bed temperature, which affects the reactions.

Selection of an adequate grid resolution, when using the multi-fluid model derived from kinetic theory of gases continues to be a major challenge. Dinh [28] argued that the multi-fluid model approach is ill-posed mathematically, since the resulting equations are non-hyperbolic, non-linear and non-conservative. They point out that the length scale disparity between the discontinuity at the phasic interface and grid resolution can be of many order of magnitude. Since the averaging process, can lead to loss of phase distribution information, it becomes necessary to refine the mesh, in order to reduce the amount of information lost. However, they point out that mesh refinement beyond the smallest cluster length scale is meaningless and can lead to nonphysical results. Fullmer [29] points out that in a dilute gas-solid flow, grid spacing as small as 10 particle diameters is required for numerical accuracy. The grid requirement becomes even more demanding in dense flow regimes, where grid spacing as low as particle diameter may be required for numerical accuracy [29]. This poses a great challenge when the size of the particle of interest is in the order of few hundred microns, as it is the case in most reacting coal gasifiers. Under such circumstances, the number of grid cells required to adequately resolve flow structures can easily reach many millions of cells. The problem becomes even more challenging, since small time-steps are needed to resolve the temporal scales of this highly unsteady flow.

The gasification reaction rates, which were obtained from the computer software PC Coal Lab required calibration. The calibration process compares the char conversion history of the coal being studied, with the char conversion history of similar coal types in PC Coal Lab database and make the appropriate adjustments to the pre-exponent constant in the rate expression. Since no char conversion history was available for the lignite coal used in the current study (i.e., the coal from Boundary Dam mine in Saskatchewan, Canada), we considered the pre-exponent constant in the gasification reaction rate as an uncertain model parameter. The uncertainty was characterized by multiplying the pre-exponent kinetic constant in the gasification reaction rate by a constant (α), since the gasification reaction rates given in Table 7 were expected to be too high.

The experimental baseline condition, where particle diameter was 285 μm and coal flow rate was 0.0495 g/s was selected for the grid study. For all simulations, second order spatial discretization and first order temporal discretization were selected. The first simulation campaign investigated the effect of grid resolution, with two uncertain input parameters, which were the ratio of steam to oxygen in the fluidized bed gasifier and the gasification reaction rates, α in Eqs. (28) and (29). Space filling Optimal Latin Hypercube (OLH) sampling technique [30] was used to generate 30 samples, where steam to oxygen ratio varied between 0.5 and 1 and the multiplier to the gasification reaction rate varied between 0.1 and 0.5, with both assumed to have a uniform distribution. The sample size for a space filling DOE coupled with a Gaussian Process model is generally determined through a heuristic measure of 10 times the number of input variables. Although there are no guarantees for convergence, it is widely accepted by experts from observing results for several applications ([31], [32]). Considering the overall extensive computational resource requirements of transient reacting multiphase flow simulations, we followed the accepted heuristic for our initial sample size. The statistical convergence is estimated using the quality of the model generated. In this case, the models can be seen to be accurate within the required criteria.

Ψ	Grid Spacing (mm)	Number of Grid Cells in I, J and K direction
35	10	15 x 175 x 15
18	5	30 x 350 x 30
9	2.5	60 x 700 x 60

Table 11 Computational grid size.

Table 11 shows the grid properties for the three grid resolutions used in this study. Based on the simulation timings recorded, 100 seconds of simulation time at grid spacing to coal particle diameter of 35, 18 and 9 takes 30, 125 and 205 days respectively on 128 cores at Ψ=35 and Ψ=18 and 256 cores at Ψ=9. The time history of the quantities of interest (e.g., CO, H_2 mole fractions), which are spatially averaged at the monitor location corresponding to the experiments is written out in a separate file during the runs. These CFD simulation results were post-processed to extract the quantities of interest from 30 sampling simulation utilizing Python scripts to perform time averaging for the last 10 seconds of each simulation. A separate sensitivity analysis for the temporal averaging duration was performed for several durations and averaging for the last 10 seconds were determined to be adequate. The temporally averaged results are then compiled in a tabulated format such a way that OLH based design of experiments matrix for the simulations performed and the corresponding quantities of interest are provided as input for the GEBHM analysis. As presented in the previous sections, the first step in the GEBHM framework is to construct a Gaussian Process Model (a.k.a. emulator) of the responses. The GPM model is then employed to conduct several UQ related analysis.

In their experimental work, Karimipour et al [3] carried out their experiment with three distinct particle sizes of 70 μm, 285 μm and 500 μm. The grid requirement of maintaining a grid size to

particle diameter (Ψ) of 10 for smaller particle diameters will make such simulations computationally very costly due to extensive resources required and impractical. In this study, the baseline experiment, with coal particle diameter of 285 μm, initial coal density of 1100 kg/m^3, composition of %41 carbon, %35 volatile matter, %10 moisture and %14 ash and coal flow rate of 0.0495 g/s was selected for simulation. Humidified air (%19.6 O_2, %16.7 H_2O and %63.7 N_2) at a rate of 0.189 g/s and temperature of 750 C enters the gasifier. The primary motivation for the selection of the baseline case among the other remaining 14 operating conditions was due to the fact that baseline case had 5 repeat experiments of the same flow conditions, which provided an assessment on the experimental uncertainties. All of the simulations for the grid resolution effect study were conducted using NETL's Joule supercomputer. Joule comprises of 1,512 nodes, where each node has two 8-core 2.6 GHz Intel Sandy Bridge CPUs for a total of 24,192 cores. Joules is a Linux based HPC cluster system, running SUSE 11.4 operating system.

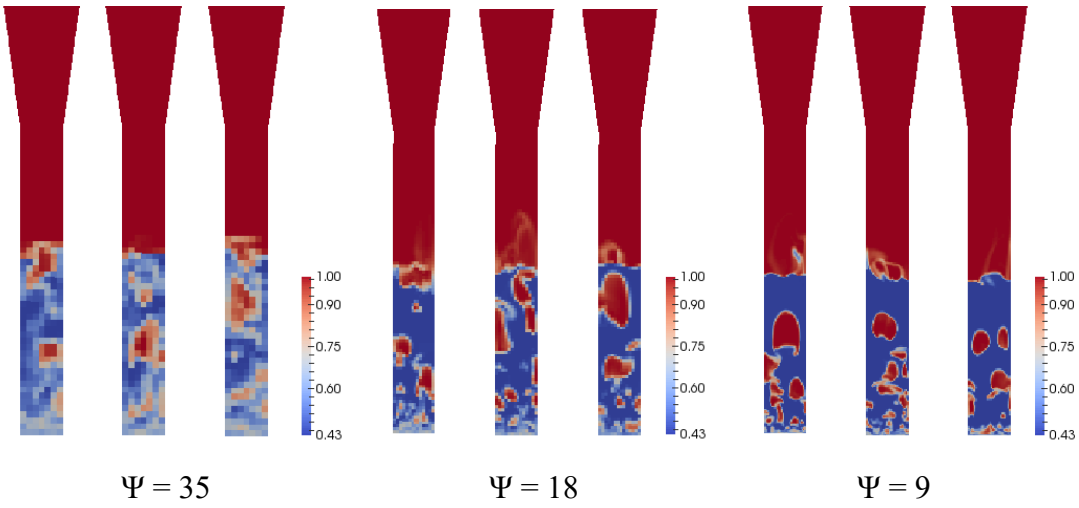

Figure 33 Snap shots of the instantaneous voidage at two different time for three mesh resolution.

The effect of computational grid on the hydrodynamics of the fluidized bed is shown in Figure 33, which shows snapshot contour images of the instantaneous voidage along the gasifier height at two different times during the simulations for three grid resolution of Ψ=35, Ψ=18 and Ψ=9. Bubble shapes are not as well defined at low grid resolution, however, as grid resolution increases, the bubble shapes become more resolved and well defined.

	H_2O/O_2 = 0.5			H_2O/O_2 = 1.0		
Grid resolution	Ψ = 35	Ψ = 18	Ψ = 9	Ψ = 35	Ψ = 18	Ψ = 9
Steam gasification	52.0%	48.3%	44.0%	68.0%	63.0%	58.1%
CO_2 gasification	9.5%	9.0%	8.3%	5.5%	5.0%	4.5%
Char oxidation	38.5%	42.7%	47.7%	26.5%	32.0%	37.1%

Table 12 Char consumption rate in the gasifier

The regions, where the solid phases (sand plus coal) are at the packing limit of 0.57 (voidage of 0.43) are shown in dark blue in Figure 33. Increasing the grid resolution not only leads to a sharper phasic interface between the gas and solids (bubble interface), it also leads to more clustering and heterogeneity of the solid phases. Figure 34 and Figure 35 show the time averaged coal volume fraction, and sand volume fraction (averaged over the last 30 seconds of the simulation) along with their standard deviation at Ψ=35, Ψ=18 and Ψ=9 grid resolution. Larger standard deviations observed in Figure 34 and Figure 35, as grid is refined point to a more heterogeneous bed being formed as the result of mesh refinement.

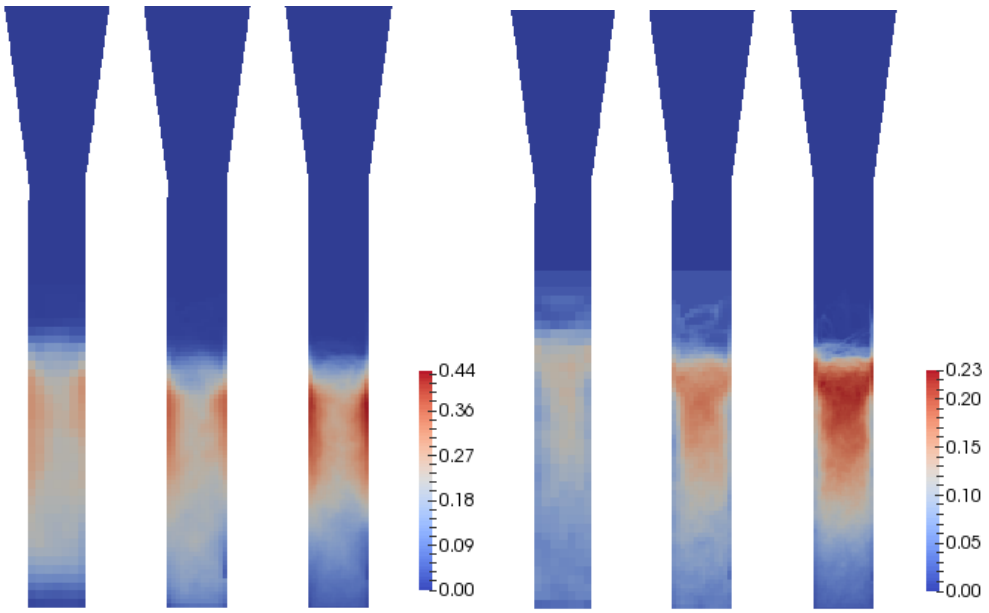

Figure 34 Time averaged coal volume fraction (left) and its standard deviation (right) at three different grid resolutions

Denser solid regions are formed throughout the bed, as mesh is refined. Regardless of mesh resolution, most of the lighter coal particles move to the top of the denser sand particles in the bed. A visual comparison of the bed height in Figure 34 and Figure 35 shows a similar bed height at grid resolutions of Ψ=18 and Ψ=9. Similar bed expansion between the medium and fine mesh resolutions indicates the hydrodynamics of the bed is not greatly affected by the mesh refinement between medium and fine mesh resolutions. To further investigate this, the Fast Fourier Transform (FFT) analysis of the CO mole fraction signal was performed, which is presented in Figure 36. The frequency spectrum for the medium and fine mesh resolutions are very similar with a dominant frequency of about 25 Hz. From Figure 36 and the similar bed expansion observed earlier, it can be concluded that no appreciable change is taking place in the hydrodynamic behavior of the fluidized bed, when grid is further refined from Ψ=18 to Ψ=9.

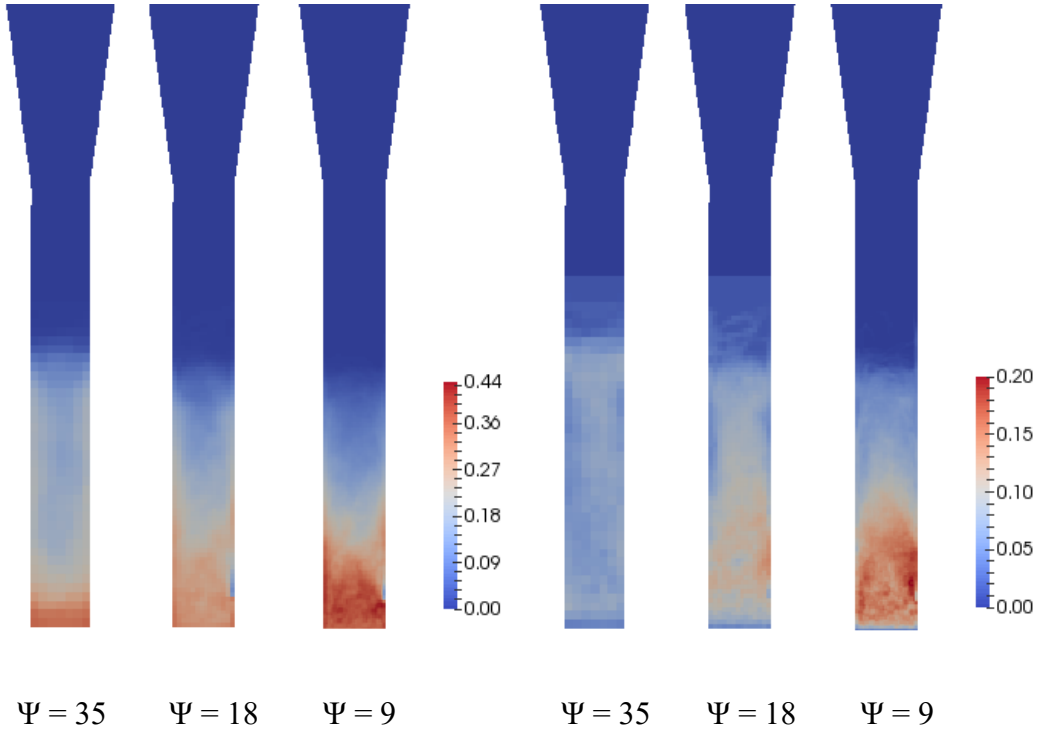

Figure 35 Time averaged sand volume fraction (left) and its standard deviation (right) at three different grid resolutions

The effect of grid refinement on the reaction models is investigated by examining average char consumption rate in the gasifier for the three grid resolutions under consideration. Table 12 shows the percentage of char consumption rate (kmole/s) in the entire gasifier due to the three-heterogeneous steam gasification, char oxidation and carbon dioxide gasification reactions at inlet steam to oxygen ration of 1.0 and 0.5 for three grid resolutions studied.

Regardless of the steam to oxygen ratio level, grid refinement leads to a decrease in overall char consumption due to gasification reactions in the reactor and an increase in char consumption due to oxidation. Although further mesh refinement beyond the medium mesh resolution does not affect the hydrodynamics of the fluidized bed, it is evident from Table 12 that gasification reactions and char oxidation reaction continue to be significantly affected by mesh refinement beyond medium mesh resolution. The reason for continued dependency of heterogeneous char reactions on the grid resolution is improvements seen in the phasic interface, when grid is refined. Figure 37 shows a snap shot of the voidage, mass fraction of steam and CO_2 in the flow. Some of the strongest reaction rates occur at the interface of bubbles, which carry the gasification agents and solid phase (coal particles), as seen in Figure 37(D) and (E). An under-resolved phasic interface leads to over-prediction of the heterogeneous reactions, since the smearing of the interface causes a higher contact area between the gas and solid. This poses a unique challenge with respect to selecting an appropriate grid resolution to carry out the simulations for routine analysis and also for non-intrusive uncertainty quantification analysis, which requires many sampling simulations. The choice of grid spacing to particle diameter ratio of 18 is adequate resolution to capture the hydrodynamics of the fluidized bed. However, the choice of grid spacing to particle diameter of 9 should provide adequate resolution (among the three-grid resolution tested) to resolve the phasic interface and capture the heterogeneous reactions taking place. Figure 38 through Figure 40 show the behavior for H_2 with respect to changes in steam to oxygen ratio and gasification rate constant for the three-grid resolution studied (Ψ=35, Ψ=18 and Ψ=9, respectively). The color legend in the figures represent the uncertainty in the emulator prediction. The uncertainty is higher, where number of samples are not adequate (such as the perimeter of the sampling space). It is clear that the general behavior of H_2 in syngas does not change with grid resolution, in the entire parametric space, which was considered in this work (response surfaces for CO and CO_2 are not shown here, since they exhibit similar behavior). Over-prediction of H_2 mass fraction when grid resolution is low is expected since the phasic interface is not resolved as well as it can be at higher mesh resolution. Since the general trend in syngas species does not change with mesh refinement and the fact that achieving 100 seconds of simulation time for Ψ=35, Ψ=18 and Ψ=9 on 128 cores, requires 30, 125 and 417 days respectively, practical considerations dictates the use of coarse grid resolution Ψ=35 for the remainder of this work.

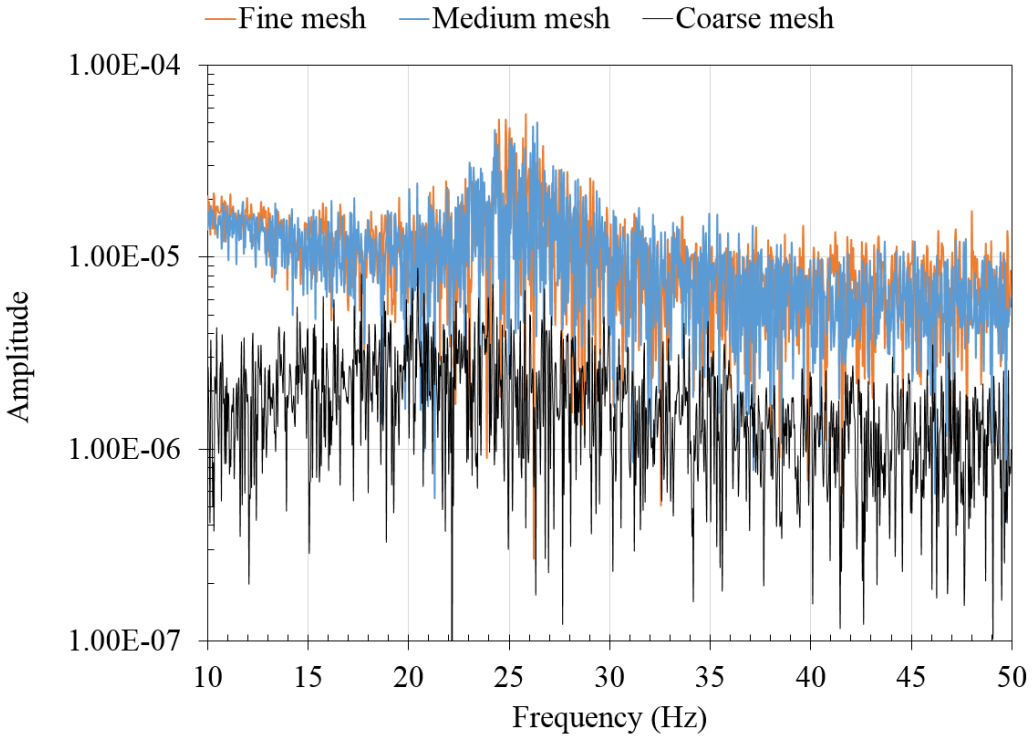

Figure 36 Frequency spectrum of CO mole fraction at three grid resolutions

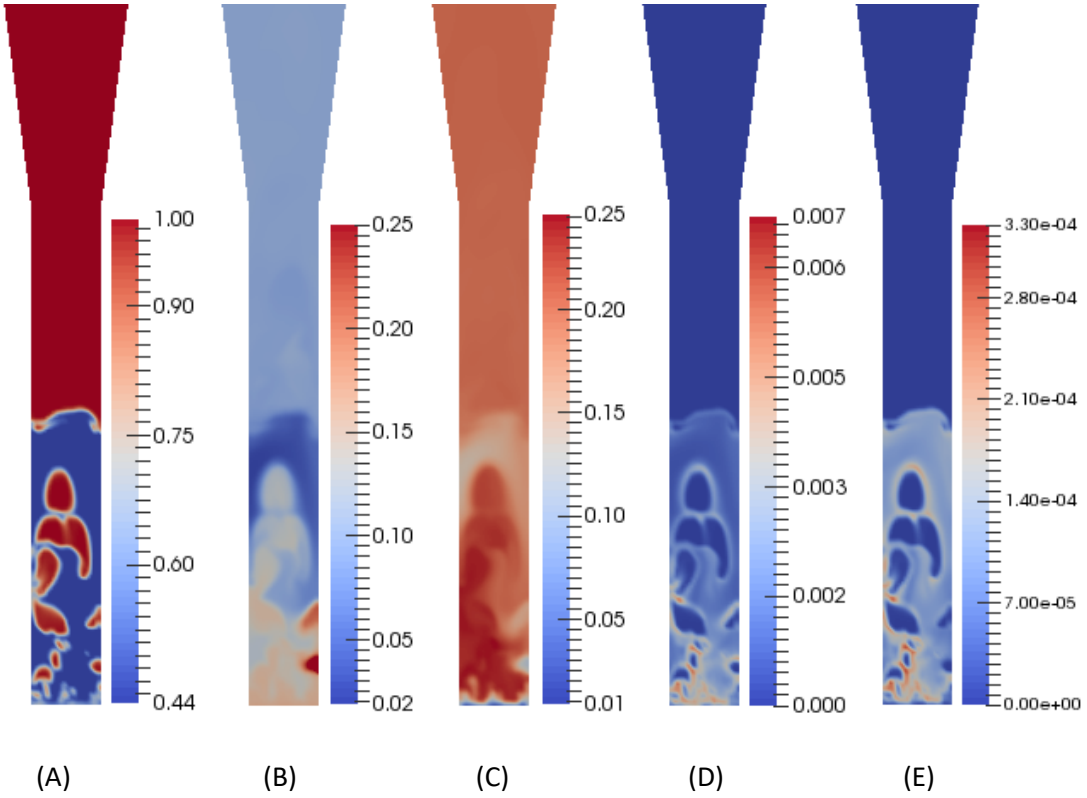

Figure 37 Instantaneous contours of (A) voidage, (B) steam mass fraction, (C) CO_2 mass fraction, (D) steam gasification rate and (E) CO_2 gasification rate.

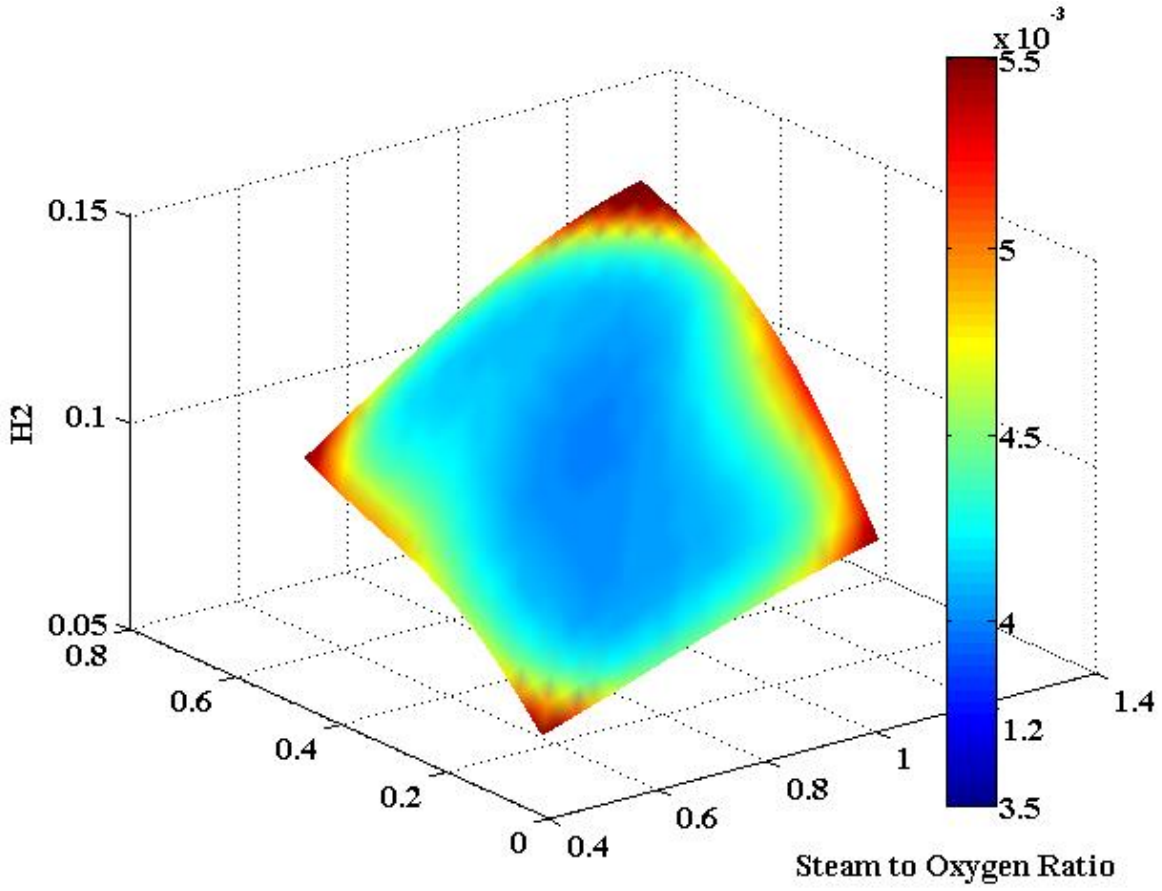

Figure 38 H_2 behavior at $\Psi = 35$ as a function of steam to oxygen ratio and multiplier to pre-exponent kinetic constant in gasification reaction model

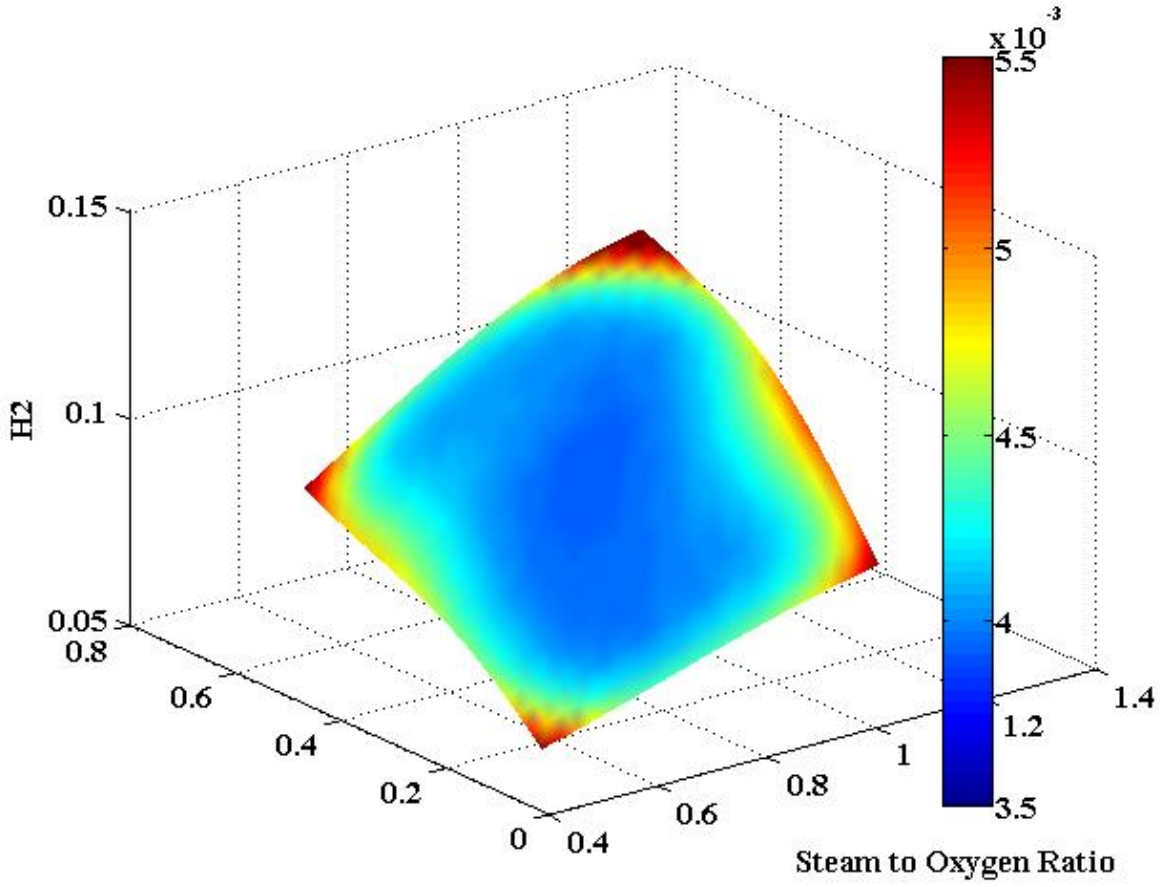

Figure 39 H_2 behavior at $\Psi = 18$ as a function of steam to oxygen ratio and multiplier to pre-exponent kinetic constant in gasification reaction model

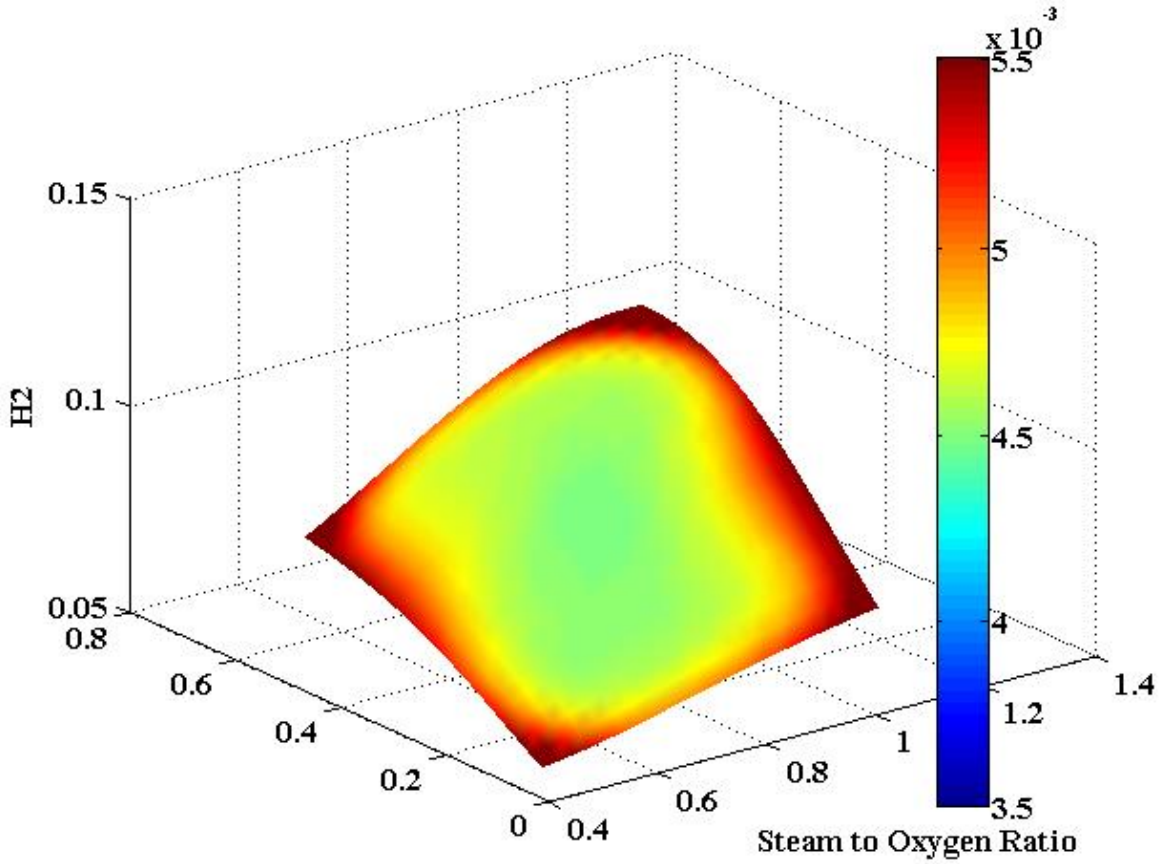

Figure 40 H_2 behavior at $\Psi = 9$ as a function of steam to oxygen ratio and multiplier to pre-exponent kinetic constant in gasification reaction model

5.5 BAYESIAN CALIBRATION

The Bayesian calibration technique, which was discussed earlier was used to calibrate the multiplier to the gasification reaction rate, which is an unobservable model parameter in MFIX-TFM simulations. The 30 OLH samples from the simulations at the Ψ=35 grid resolution were used. The prior distribution for this multiplier was assumed to be uniform and varying between a range of 0.1 to 0.5. GEBHM uses Markov Chain Monte Carlo (MCMC) to compute the posterior distribution of calibration parameters and compute the hyperparameters of the Gaussian Process models. 10,000 MCMC steps with an additional 5,000 burn-in steps were used to compute the posterior distributions. The posterior distribution of the calibration parameter obtained from GEBHM is shown in Figure 41, with a median value of 0.2254 and standard deviation of 0.03524. Figure 42 illustrates the CFD results for CO mole fractions with the multiplier to the gasification reaction rates set to the calibrated value of 0.2254 and also set to the default value of 1.0 (uncalibrated) at grid resolution of Ψ=35. Although the calibrated gasification reaction rate multiplier of 0.2254 is the most probable value for improving the simulation results, the calibrated CFD results do not show the correct trend, when compared with the experimental values at steam to oxygen ratio of 0.5, 0.75 and 1.0. This is attributed to the systematic discrepancy that exists in the CFD simulations. The discrepancy adjusted predictions from GEBHM provide a closer look at the systematic discrepancy observed in the CFD simulation results. The optimal Latin hypercube based 30 sampling simulations at grid resolution of Ψ=35 are shown as gray dots in the same figure. Large discrepancies exist, when comparing the experimental results to both un-calibrated and calibrated results. However, once the calibrated emulator results are corrected for the discrepancy term by GEBHM, good agreement is achieved with experimental data, as seen in Figure 42. This clearly shows that the discrepancy model obtained from GEBHM is sufficient for correcting the missing effects in the simulator and the calibration parameter has not been over-tuned to fit the experimental observations

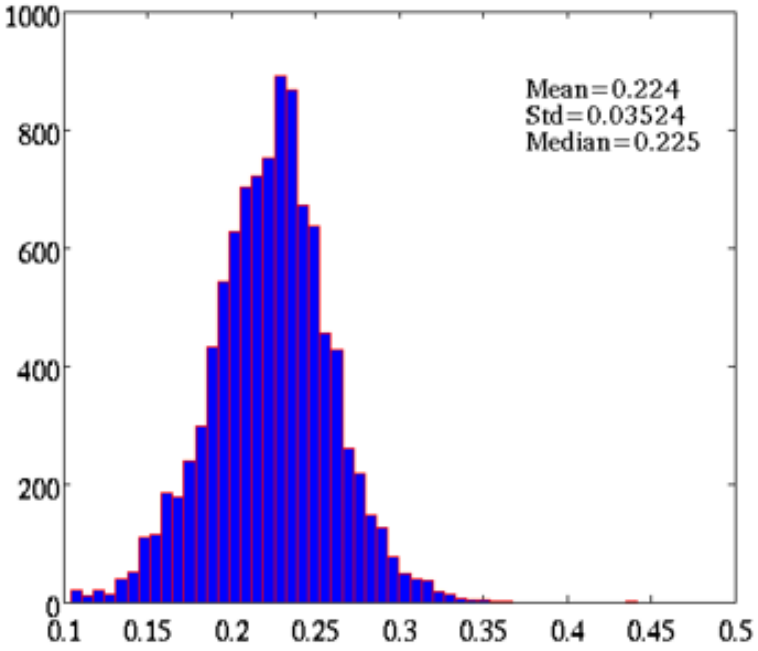

Figure 41 Posterior distribution of the multiplier to gasification rate, after Bayesian calibration

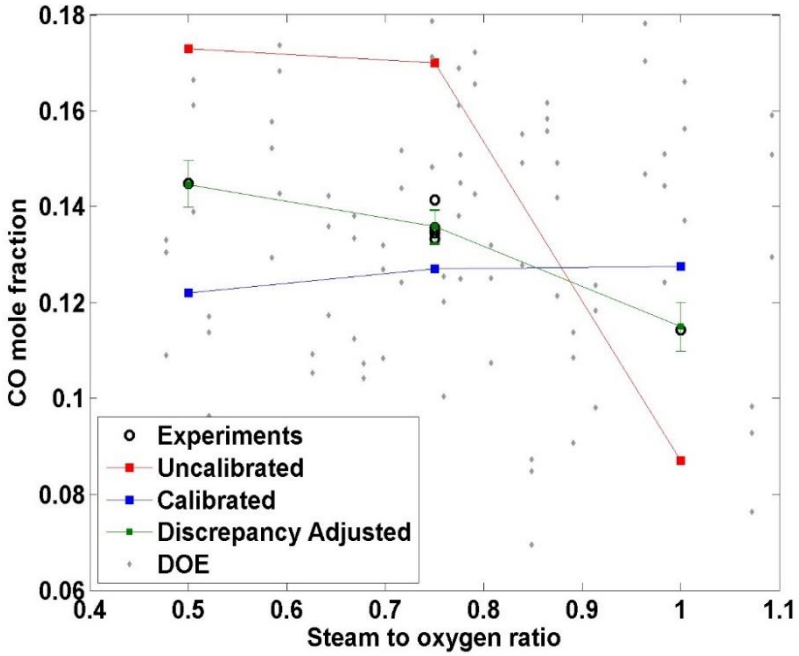

Figure 42 CO mole fraction predictions for calibrated and un-calibrated gasification reaction rate.

6. CONCLUSION

The application of non-intrusive Bayesian uncertainty quantification methodology for multiphase reacting flow is demonstrated by utilizing an existing experimental dataset and conducting CFD simulations of the conditions used in the experiment. The choice of input parameters, quantities of interest variables, sampling technique and number of samples were considered fixed and kept as the same due to the prior experimental work carried out by Karimipour et al. [3]. One of the contributions of the current work is the new set of emulators (i.e., surrogate models) constructed for the quantities of interests based on species mole fractions (e.g., CO, CO_2 and H_2 mole fractions) instead of derived quantities (e.g., gasification efficiency) or ratios of mole fractions as presented in the original study. Emulators were constructed based on Gaussian Process Model, which also provided a detailed assessment on uncertainty of the surrogate model constructed as opposed to the polynomial regression based response surfaces constructed in the original study, which offered limited surrogate model related uncertainty assessment. The quality of the emulators was assessed before any type of UQ analysis was performed as the emulator plays critical role in the present approach. As part of the UQ assessment, global sensitivity analysis was performed on the experimental data of Karimipour et al. [3], which showed that the third factor, i.e., steam to oxygen ratio is the primary uncertain input parameter that affects the variability observed in the syngas composition. This finding is similar to what Karimipour et al. [3] reported. However, the methodology followed in this paper also indicates that the sensitivity observed in steam to oxygen ratio is directly affected by coal flow rate and particle size (the other two uncertain inlet parameters), even though coal flow rate and particle size do not directly affect the syngas composition. Another UQ analysis performed was the forward propagation of input uncertainties by characterizing them with several probability density distribution functions. The results showed that the probability density distribution form of the inlet uncertain parameters does not affect the syngas composition. The surrogate models constructed can also be employed in providing guidance on trends and relationships between input and output parameters in addition to their critical role in UQ analysis. Using the emulator generated as part of the UQ study, the question of what additional sampling points would improve the surrogate model uncertainty was also investigated by framing the question as an optimization problem. For demonstration purposes a single objective optimization to determine sampling location that maximizes the uncertainty in the surrogate model was solved using global multi-point particle swarm optimization. Ten additional sampling points were determined, which were identified to be the best points to conduct a new set of experiments to maximize information gain and thus minimize uncertainty.

The effect of grid resolution in CFD simulations of the fluidized bed gasifier of Karimipour et al. [3] was studied next. A grid spacing of 18 times larger than the particle diameter was sufficiently resolved to capture the hydrodynamic of the fluidized bed (no appreciable change in bed height and frequency spectrum were observed between $\Psi = 18$ and $\Psi = 9$). However, a grid spacing of at least 9 times larger than particle diameter was needed for capturing the syngas species field. This is due to an under-resolved phasic interface (where the strongest heterogeneous reactions take place) at larger grid spacing. Conducting uncertainty quantification based on either of the grid sizes mentioned above is computationally costly and impractical. It was observed that grid spacing of 35 times larger than the particle diameter will yield the same

trends and overall behavior by the species field than finer grid spacing, although the gasification reaction is over-predicted and char oxidation reaction is under-predicted, when comparing results between $\Psi = 35$ and $\Psi = 9$. Due to the fact that physical run time for simulations conducted at $\Psi = 35$ grid resolution were 14 times faster than simulations conducted at $\Psi = 9$ grid resolution, grid spacing of 35 times the particle diameter was chosen as the grid spacing used for the additional UQ analysis that was conducted.

The global sensitivity analysis of simulations based on the experimental condition shows that the predicted syngas composition is strongly affected not only by the steam to oxygen ratio (which was observed in the experiments as well) but also by variation in the coal flow rate and particle diameter (which was not observed in the experiments). The CO mole fraction is underpredicted at lower steam-to-oxygen ratios and overpredicted at higher steam-to-oxygen ratios. The opposite trend is observed for the CO2 mole fraction. These discrepancies are attributed to either (i) excessive segregation of the phases, which leads to the fuel-rich or -lean regions, where homogeneous and heterogeneous reactions can over- or underproduce the product gases, or (ii) selection of the reaction models, where different reaction models and kinetics can lead to different syngas compositions throughout the gasifier.

A closer study into the effect of reaction models on syngas composition shows that among the reaction models for water gas shift, gasification, char oxidation, the choice of reaction model for water gas shift has the greatest influence on syngas composition, with gasification reaction model being second. Syngas composition also shows a small sensitivity to temperature of the bed.

As non-intrusive uncertainty quantification assessment heavily relies on the number of sampling simulations performed, external high performance computing resources were sought in addition to the NETL high performance computing resources. For this purpose, two ASCR Leadership Computing Challenge (ALCC) program awards from the U.S. Department of Energy's Office of Science were secured through a competitive proposal submission and award process. Proposal submitted for the 2014 ALCC program led to 38 million CPU hour award at the National Energy Research Scientific Computing Center (NERSC). In the following year, under the 2015 ALCC program, 111.5 million CPU hour were awarded at the Argonne Leadership Computing Facility (ALCF) in Argonne National Laboratory of the U.S. Department of Energy. The findings from series of studies conducted were compiled and published in three journal papers, Gel et al. [7], [13] and Shahnam et al. [33].

The insight gained from the current study for the bench-scale fluidized bed gasifier, has played an important role in our computational modeling efforts where there are not only the physical operating factors such as coal flow rate or steam to oxygen ratio but also number of modeling parameters, which requires careful consideration for uncertainty quantification assessment of computational fluid dynamics simulations of multiphase flows.

7. REFERENCES

[1] "Strategic center for coal at national energy technology laboratory (netl)".

[2] "Report on workshop on multiphase flow research, Tech. Rep. DOE/NETL-2007/1259," National Energy Technology Laboratory of U.S. Department of Energy, Morgantown, WV, June 2006.

[3] Karimipour, S., Gerspacher, R., Gupta, R. and Spiteri, R.J., "Study of factors affecting syngas quality and their interactions in fluidized bed gasification of lignite coal," *Fuel,* vol. 103, pp. 308-320, 2013.

[4] S. Karimipour, "Private communication regarding raw experimental dataset," Calgary, Canada, 2013.

[5] "NETL Multiphase Flow Science, MFIX Software Suite website," http://mfix.netl.doe.gov, 2016.

[6] Lane, W.A., Storlie, C.B., Montgomery, C.J. and Ryan, E.M., "Numerical modeling and uncertainty quantification of a bubbling fluidized bed with immersed horizontal tubes," *Powder Technology,* vol. 253, pp. 733-743, 2014.

[7] Gel, A., Shahnam, M. and Subramaniyan, A.K., "Quantifying uncertainty of a reacting multiphase flow in a bench-scale fluidized bed gasifier. A Bayesian approach," *Powder Technology,* vol. 311, pp. 484-495, 2017.

[8] Myers, R.H., Montgomery, D.C. and Anderson-Cook, C.M., Response surface methodology: process and product optimization using designed experiments, John Wiley & Sons, Vol. 705, 2009.

[9] Kennedy, M.C. and O'Hagan, A., "Bayesian calibration of computer models," *Journal of the Royal Statistical Society: Series B (Statistical Methodology),* vol. 63, pp. 425-464, 2001.

[10] Subramaniyan, A. K., Wang, L., Beeson, D., Nelson, J., Berg, R. and Cepress, R., "A comparative study on accuracy and efficiency of metamodels for large industrial datasets," *ASME 2011 Turbo Expo: Turbine Technical Conference and Exposition, American Society of Mechanical Engineers,* pp. 759-769, 2011.

[11] Subramaniyan, A. K., Kumar, N. C. and Wang, L., "Probabilistic validation of complex engineering simulations with sparse data," in *ASME Turbo Expo 2014: Turbine Technical*

Conference and Exposition, American Society of Mechanical Engineers, V07BT30A003–V07BT30A003, 2014.

[12] Higdon, D., Kennedy, M., Cavendish, J., Cafeo, J. and Ryne, R.D., "Combining field observations and simulations for calibration and prediction," *SIAM Journal of Scientific Computing*, vol. 26, pp. 448-466, 2004.

[13] Gel, A., Shahnam, M., Musser, J, Subramaniyan, A.K. and Dietiker, J.F., "Non-intrusive Uncertainty Quantification of Computational Fluid Dynamics Simulations of a Bench-scale Fluidized Bed Gasifier," *Industrial & Engineering Chemistry Research*, no. DOI: 10.1021/acs.iecr.6b02506, 2016.

[14] Holloway, J.P., Bingham, D.C., Chuan-Chih, Doss, F., Drake, R.P., Fryxell, B., Grosskopf, M., Van der Holst, B., Mallick, B.K. and McClarren, R., "Predictive modeling of a radiative shock system," *Reliability Engineering & System Safety*, vol. 96, pp. 1184-1193, 2011.

[15] Roy, C.J. and Oberkampf, W. L., "A comprehensive framework for verification, validation, and uncertainty quantification in scientific computing," *Computer Methods in Applied Mechanics and Engineering*, vol. 200, pp. 2131-2144, 2011.

[16] Gel, A., Garg, R., Tong, C., Shahnam, M., and Guenther, C., "Applying uncertainty quantification to multiphase flow computational fluid dynamics," *Powder Technology*, vol. 242, pp. 27-39, 2013.

[17] Syamlal, M., Rogers, W. and O'Brien, T. J., "MFiX documentation theory guide," https://mfix.netl.doe.gov/.

[18] Benyahia, S., Syamlal, M., and O'Brien, T.J.;, "Summary of MFiX equations," 2012.

[19] S. Niksa, "PC Coal Lab version 4.1: user guide and tutorial," Niksa Energy Associates LLC, Belmont, CA, 1997.

[20] Field, M., Gill, D., Morgan, B. and Hawksley, P., "Combustion of Pulverized coal," in *British Coal Utilisation Research Association (BCURA)*, Leatherhead, England, 1967.

[21] DeSai, P. and Wen, C., Computer modeling of merc's fixed bed gasifier, 1978.

[22] J. Howard, "Fundamentals of coal pyrolysis and hydropyrolysis," *Chemistry of coal utilization, Second Supplementary Volume*, pp. 665-784, 1981.

[23] Westbrook, C.K., Dryer, F.L, "Simplified reaction mechanisms for the oxidation of hydrocarbon fuels in flames," in *Combustion science and technology*, 27, 1-2, 1981.

[24] N. Peters, "Premixed burning in diffusion flames—the flame zone model of libby and economos," *International Journal of Heat and Mass Transfer*, vol. 22, pp. 691-703, 1979.

[25] Dryer, F.L., Glassman, I., "14th International Symposium on Combustion, High Temperature Oxidation of CO and CH4," in *The Combustion Institute*, 1973.

[26] Chen, W., Sheu, F., and Savage, R., "Catalytic activity of coal ash on steam methane reforming and water-gas shift reactions," *Fuel processing technology*, pp. 279-288, 16, 1987.

[27] Biba, V., Macak, J., Klose, E., and Malecha, J., "Mathematical model for the gasification of coal under pressure," *Industrial & Engineering Chemistry Process Design and Development*, pp. 92-98, 17, 1978.

[28] Dinh, T., Nourgaliev, R., and Theofanous, T., "Understanding the ill-posed two-fluid model," in *The 10th International Topical Meeting on Nuclear Reactor Thermal Hydraulics NURETH10*, South Korea, 2003.

[29] Fullmer, W. and Hrenya, C., "Quantitative assessment of fine-grid kinetic theory based predictions of mean-slip in unbounded fluidization," *AIChE Journal*, Vols. DOI 10.1002/aic, 62, no. 2016, pp. 11-17.

[30] J. Park, "Optimal Latin-hypercube designs for computer experiments," *Journal of statistical planning and inference*, vol. 39, pp. 95-111, 1994.

[31] Forrester, A., Sobester, A. and Keane, A., Engineering design via surrogate modelling: a practical guide, John Wiley & Sons, 2008.

[32] Koziel, S. and Leifsson, L., "Surrogate-based modeling and optimization," *Applications in Engineering*, 2013.

[33] Shahnam, M., Gel, A., Dietiker, J.-F., Subramaniyan, A. K. and Musser, J., "The Effect of Grid Resolution and Reaction Models in Simulation of a Fluidized Bed Gasifier through Non-intrusive Uncertainty Quantification Techniques," *ASME Journal of Verification, Validation and Uncertainty Quantification*, 2016.

Sean Plasynski
Executive Director
Technology Development & Integration Center
National Energy Technology Laboratory
U.S. Department of Energy

John Wimer
Associate Director
Strategic Planning
Science & Technology Strategic Plans & Programs
National Energy Technology Laboratory
U.S. Department of Energy

David Allman
Executive Director
Research & Innovation Center
National Energy Technology Laboratory
U.S. Department of Energy